

Mathematical methods for neutrino cross-section extraction

Steven Gardiner*

Fermi National Accelerator Laboratory, Batavia, Illinois 60510 USA

(Dated: January 9, 2024)

Precise modeling of neutrino-nucleus scattering is becoming increasingly important as accelerator-based oscillation experiments seek definitive answers to open questions about neutrino properties. To guide the needed model refinements, a growing number of experimental collaborations are pursuing a wide-ranging program of neutrino interaction measurements at GeV energies. A key step in most such analyses is cross-section extraction, in which measured event counts are corrected for background contamination and imperfect detector performance to yield cross-section results that are directly comparable to theoretical predictions. In this paper, I review the major approaches to cross-section extraction in the literature using representative examples from the MINERvA, MicroBooNE, and T2K experiments. I then present two mathematical techniques, blockwise unfolding and the conditional covariance background constraint, which overcome some limitations of typical cross-section extraction procedures.

I. INTRODUCTION

At the GeV energies relevant for accelerator-based neutrino oscillation experiments, there is increasing theoretical and experimental investment toward achieving a precise understanding of the physics of neutrino interactions with atomic nuclei [1]. This effort is intended to maximize the discovery potential of large, next-generation experiments like Hyper-Kamiokande [2] and DUNE [3], which will need percent-level control of systematic uncertainties to successfully execute their flagship analyses [4].

A rapidly growing literature of neutrino cross-section measurements is serving as an indispensable resource for benchmarking calculations and improving nuclear theory and simulations to the needed level. Due to the broad range of energies produced in accelerator neutrino beams and the difficulty of accurately reconstructing the incident neutrino energy on an event-by-event basis, the majority of modern neutrino scattering measurements are presented as flux-averaged differential cross sections.¹ These may generally be written in the form

$$\left\langle \frac{d^n\sigma}{d\mathbf{x}} \right\rangle \equiv \frac{1}{\Phi} \int \varphi(E_\nu) \frac{d^n\sigma(E_\nu)}{d\mathbf{x}} dE_\nu, \quad (1)$$

where

$$\Phi \equiv \int \varphi(E_\nu) dE_\nu \quad (2)$$

is the integral of the beam flux $\varphi(E_\nu)$ over neutrino energy E_ν , and $d^n\sigma(E_\nu)/d\mathbf{x}$ is the energy-dependent differential cross section as a function of n kinematic variable(s) \mathbf{x} of interest.

The usual starting point for a neutrino cross-section analysis involves defining the signal event topology and

the observable(s) \mathbf{x} to be measured. Based upon these choices, event selection criteria are developed to isolate signal events from background. A binning scheme is also specified in which selected events belonging to distinct ranges of the observables are tallied separately from each other. Due to limited detector resolution, some events will inevitably be assigned to an incorrect bin. The impact of these bin migrations is estimated using simulation and typically quantified using two separate sets of bins. The *true bins* are defined in terms of the actual values of the observables, while the *reconstructed bins* collect events whose measured values fall within an appropriate range.

The final step of a neutrino scattering analysis is known as *cross-section extraction* and involves correcting the observed event counts in each reconstructed bin for remaining background, detector efficiency, and bin migrations. Scaling factors are then applied to the corrected event counts to obtain cross sections that can be compared to interaction model predictions.

While important and sometimes subtle differences exist in the cross-section extraction procedures used by different experimental collaborations, nearly all strategies currently in use can be expressed in the form

$$\left\langle \frac{d^n\sigma}{d\mathbf{x}} \right\rangle_\mu = \frac{\sum_a U_{\mu a} (D_a - B_a)}{\Phi T \Delta \mathbf{x}_\mu}. \quad (3)$$

Here the symbol D_a (B_a) represents the total number of measured events (estimated number of background events) in the a -th reconstructed bin.

The elements $U_{\mu a}$ of the *unfolding matrix* are used to apply efficiency and bin migration corrections to the background-subtracted event counts. They may equivalently be written as

$$U_{\mu a} = \frac{P_{\mu a}}{\epsilon_\mu}, \quad (4)$$

where ϵ_μ is the detection efficiency for signal events belonging to the μ -th true bin, and $P_{\mu a}$ is the conditional

* gardiner@fnal.gov

¹ As noted in a recent review [5], the term *flux-integrated* is also commonly used in the literature, typically with an equivalent meaning.

probability that a signal event measured within the a -th reconstructed bin also belongs to the μ -th true bin. In this paper, Greek subscripts (μ, λ) are used to represent true bin indices, while Latin subscripts (a, b) represent reconstructed bin indices.

The denominator from Eq. 3 contains the scaling factors needed to convert the unfolded signal event count into a differential cross section. The symbol T denotes the number of scattering targets illuminated by the neutrino beam and included in the active region of the detector used to measure the reconstructed event counts D_a . Expressing T as a number of target atoms or a number of target nucleons are both common conventions in the literature. The symbol $\Delta\mathbf{x}_\mu$ represents the product of the n bin widths for the μ -th true bin.

The resulting differential cross section on the left-hand side of Eq. 3 is an average value in the μ -th true bin. If this bin is defined so that it contains all signal events with values of the observables \mathbf{x} such that

$$\mathbf{x} \in [\mathbf{x}_\mu, \mathbf{x}_{\mu+1}), \quad (5)$$

then the average cross section in this bin may be written in terms of the definition given in Eq. 1 as

$$\left\langle \frac{d^n\sigma}{d\mathbf{x}} \right\rangle_\mu \equiv \frac{1}{\Delta\mathbf{x}_\mu} \int_{\mathbf{x}_\mu}^{\mathbf{x}_{\mu+1}} \left\langle \frac{d^n\sigma}{d\mathbf{x}} \right\rangle d\mathbf{x}. \quad (6)$$

The n -dimensional limits \mathbf{x}_μ and $\mathbf{x}_{\mu+1}$ define the region of kinematic phase space spanned by the bin.

II. CURRENT APPROACHES

Significant variations exist between the approaches to cross-section extraction employed in modern neutrino experiments. While the basic concepts described in the introduction are essentially universal, key differences exist between the methods used to estimate unfolding corrections and to compute uncertainties on the extracted measurement. To provide sufficient context for the mathematical techniques presented in later sections of this paper, three representative cross-section extraction strategies from the MINERvA, MicroBooNE, and T2K experiments are described below.

A. MINERvA-style extraction

The MINERvA collaboration has published an extensive library of flux-averaged neutrino cross sections [6–38] following a consistent extraction procedure. Unfolding corrections are evaluated using Richardson-Lucy deconvolution [39, 40], an iterative algorithm popularized in high-energy physics by D’Agostini [41]. A MINERvA-specific fork of the RooUnfold [42] software package, called UnfoldUtils [43], is coupled to the MINERvA Analysis Toolkit [44] to provide the numerical implementa-

tion.

1. D’Agostini unfolding

The starting point for the D’Agostini method is a set of initial estimators $\hat{\phi}_\mu^0$ for the unfolded signal event counts (i.e., the numerator in Eq. 3) in each of the μ true bins. These are arbitrary but typically taken from the main simulation prediction used to execute the analysis. Each iteration i of the method obtains an updated estimator

$$\hat{\phi}_\mu^{i+1} = \sum_a U_{\mu a}^i d_a \quad (7)$$

by applying the unfolding matrix from Eq. 4 to the background-subtracted measured event counts

$$d_a \equiv D_a - B_a \quad (8)$$

in each of the a reconstructed bins. While the detection efficiency ϵ_μ is held constant over iterations, the conditional probability is updated each time via the formula

$$P_{\mu a}^i = \frac{M_{a\mu} \hat{\phi}_\mu^i}{\sum_\lambda M_{a\lambda} \hat{\phi}_\lambda^i}. \quad (9)$$

Here the elements of the *migration matrix* $M_{a\mu}$ represent the probability that a measured signal event belonging to the μ -th true bin will be assigned to the a -th reconstructed bin. They are typically estimated from simulation via

$$M_{a\mu} = \frac{\phi_{a\mu}}{\sum_b \phi_{b\mu}} \quad (10)$$

where $\phi_{a\mu}$ is the number of simulated signal events belonging simultaneously to the μ -th true bin and the a -th reconstructed bin.

The total number of iterations f is typically chosen based on the unfolding performance in mock-data studies. The estimator $\hat{\phi}_\mu^f$ obtained in the last iteration is used to obtain the final cross-section result.

2. Multiple-universe extraction

Systematic uncertainties on the measurement are represented as covariance matrices that are calculated using a set of N_{univ} alternative simulations, or *universes*. In each universe u , the quantities $U_{\mu a}$, B_a , Φ , and T are calculated based upon the alternative simulation, and the cross section is re-extracted according to Eq. 3. The covariance on the resulting differential cross section is then computed as the maximum likelihood estimate assuming that the universes are drawn from a multivariate Gaus-

sian distribution:

$$\text{Cov}(s_\mu, s_\lambda) = \frac{1}{N_{\text{univ}}} \sum_{u=1}^{N_{\text{univ}}} (s_\mu^u - \bar{s}_\mu)(s_\lambda^u - \bar{s}_\lambda). \quad (11)$$

Here I have defined the abbreviation

$$s_\mu \equiv \left\langle \frac{d^n \sigma}{d\mathbf{x}} \right\rangle_\mu. \quad (12)$$

The symbol s_μ^u denotes the value of the extracted differential cross section s_μ evaluated in the u -th universe. For a single alternative universe ($N_{\text{univ}} = 1$), the symbol \bar{s}_μ represents the value of s_μ obtained using the nominal MINERvA simulation. For multiple systematic variations, \bar{s}_μ denotes the arithmetic mean of s_μ evaluated in all of the universes.

Detailed documentation for the treatment of data statistical uncertainties in the MINERvA procedure does not appear to be available in their publications. However, a bootstrapping method involving re-extraction of the cross sections s_μ in universes for which the measured event counts D_a fluctuate according to Poisson statistics has been used in a MINERvA-style analysis by NOvA [45]. Analytic propagation of the statistical covariance matrix through unfolding, as described for MicroBooNE in Sec. II B 2, would also be a reasonable approach.

3. Real-flux measurement

As discussed at length in Ref. [46], the extraction procedure adopted by MINERvA leads to a differential cross section result that is averaged over the *real* neutrino flux received by the detector. This flux differs from the *reference* flux obtained from simulation and used to compute theoretical predictions of the cross sections in a way that is not exactly known. Rigorously quantifying goodness-of-fit (e.g., via a chi-squared metric) between a cross-section calculation and the data extracted according to the MINERvA treatment therefore requires uncertainties on the flux shape as a function of neutrino energy to be evaluated on the model prediction.

4. Use by other experiments

MINERvA-like strategies for cross-section extraction are dominant in the accelerator neutrino interaction literature, with similar approaches being used in measurements by NOvA [45, 47, 48], T2K [49–57], MiniBooNE [58–64] and MicroBooNE [65]. Several cross-section analyses from ArgoNeuT and one from MicroBooNE evaluate uncertainties in the MINERvA style by re-extracting the cross section in multiple systematic universes, but bin migration corrections are either entirely neglected [66, 67] or are evaluated in a more

approximate way using effective values of the detection efficiency [68–71].

B. MicroBooNE-style extraction

In an effort to mitigate concerns about model dependence in the extraction procedure, two early MicroBooNE cross-section measurements were reported using a *forward-folding* approach [72, 73]. Under this strategy, bin migration adjustments are applied to theoretical predictions rather than the extracted data when performing quantitative comparisons. Limitations of the MicroBooNE forward-folding formalism were examined in subsequent community discussions [74] that discouraged further use. Although tools exist that would enable a more sophisticated variation of forward-folding [75], the MicroBooNE collaboration has opted to release unfolded results in all recent publications presenting differential cross sections. Most of these [76–81] employ a relatively new unfolding technique called the Wiener-SVD method [82], which was originally implemented in a dedicated code [83] based on ROOT [84, 85].

1. Wiener-SVD unfolding

The Wiener-SVD technique is built on the observation that unfolding the signal event counts may be interpreted as a likelihood optimization problem. A straightforward approach uses direct inversion of the *detector response matrix*

$$\Delta_{a\mu} \equiv \epsilon_\mu M_{a\mu} \quad (13)$$

to obtain the unfolding matrix:

$$U^{\text{direct}} = (\Delta^T \Delta)^{-1} \Delta^T. \quad (14)$$

Here the left inverse is written rather than the ordinary inverse (Δ^{-1}) to cover cases in which Δ is not a square matrix. While U^{direct} corresponds to the maximum likelihood solution to the unfolding problem, its use has known pathologies, including large uncertainties. To improve upon the direct inversion strategy, standard unfolding techniques rely upon *regularization*: new constraints are introduced into the likelihood function based on prior information about the expected solution. These are intended to reduce the variance on the unfolded result at the cost of some (hopefully small) bias.

The Wiener-SVD authors note that the impact of regularization can be written for a general unfolding matrix U in terms of the direct inversion one via

$$U = A_C \cdot U^{\text{direct}}. \quad (15)$$

Thus, an unfolding method that can be represented as a matrix transformation of the background-subtracted data, as in Eq. 3, may be expressed as a recipe for

construction of the *regularization matrix* or *additional smearing matrix* A_C . A full derivation of A_C for the Wiener-SVD method, which is based on an analogy with the Wiener filter used in signal processing, is provided in the original publication [82]. The details of the calculation are unimportant for the present discussion, but Appendix A provides a brief summary.

2. Analytic uncertainty propagation

One of the required inputs for the Wiener-SVD unfolding method is a covariance matrix $\text{Cov}(D_a, D_b)$ that includes all statistical and systematic uncertainties on the measured total event counts D_a in the reconstructed bins a . The need for this covariance matrix motivates an uncertainty treatment for MicroBooNE that is distinct from MINERVA's. The differences in the uncertainty quantification strategy are ultimately more consequential than those in the specifics of the unfolding itself.

Under the MicroBooNE approach, data statistical covariances are evaluated in the usual way for Poisson statistics. Systematic covariances are estimated using the corresponding covariances on the expected event counts n_a obtained from simulation:

$$\text{Cov}(D_a, D_b) \approx \text{Cov}(n_a, n_b). \quad (16)$$

These in turn are computed using a multiple-universe approach similar to the one in Eq. 11 from MINERVA:

$$\text{Cov}(n_a, n_b) = \frac{1}{N_{\text{univ}}} \sum_{u=1}^{N_{\text{univ}}} (n_a^u - n_a^{\text{CV}})(n_b^u - n_b^{\text{CV}}). \quad (17)$$

In this case, however, the quantity of interest is the simulation prediction for the number of events n_a in the a -th reconstructed bin, and the *central-value* prediction from MicroBooNE's nominal simulation n_a^{CV} is used in the expression rather than the mean value from the alternate universes.

A special treatment is employed for uncertainties arising from MicroBooNE's neutrino interaction model [86]. While the expected event counts n_a are varied directly in most of the systematic universes, those related to the interaction model use the expression

$$n_a = B_a + \sum_{\mu} \Delta_{a\mu} \phi_{\mu}^{\text{CV}} \quad (18)$$

in which the detector response matrix $\Delta_{a\mu}$ is applied to the central-value prediction of signal event counts in each of the μ true bins. Because uncertainties related to interaction modeling of signal events will affect cross-section extraction only through their influence on unfolding, the background B_a and the response matrix elements $\Delta_{a\mu}$ are varied in each relevant universe while the signal prediction ϕ_{μ}^{CV} is held constant. When the central-value response matrix is used, the second term in Eq. 18 is just

the nominal prediction for the number of signal events in the a -th reconstructed bin.

Since background subtraction involves shifting the content of each reconstructed bin by a constant, the covariance on the background-subtracted event counts d_a from Eq. 8 is the same as the covariance before subtraction:

$$\text{Cov}(d_a, d_b) = \text{Cov}(D_a, D_b). \quad (19)$$

Final uncertainties on the differential cross section measurement are obtained by analytically propagating the covariance matrices through the extraction procedure, which is applied only once. Using the abbreviated notation from Eq. 12, the covariance matrix describing the measurement may be written as

$$\text{Cov}(s_{\mu}, s_{\lambda}) = \frac{\text{Cov}(\hat{\phi}_{\mu}, \hat{\phi}_{\lambda})}{\Phi^2 T^2 \Delta x_{\mu} \Delta x_{\lambda}}. \quad (20)$$

Here the covariance on the unfolded signal event counts

$$\hat{\phi}_{\mu} = \sum_a U_{\mu a} d_a \quad (21)$$

is computed via

$$\text{Cov}(\hat{\phi}_{\mu}, \hat{\phi}_{\lambda}) = \sum_{a,b} \mathfrak{E}_{\mu a} \text{Cov}(d_a, d_b) \mathfrak{E}_{b\lambda}^T. \quad (22)$$

In general, the elements of the *error propagation matrix* \mathfrak{E} are the partial derivatives

$$\mathfrak{E}_{\mu a} \equiv \frac{\partial \hat{\phi}_{\mu}}{\partial d_a}. \quad (23)$$

For Wiener-SVD and similar methods where the unfolding matrix does not depend on the data, this becomes simply

$$\mathfrak{E}_{\mu a} = U_{\mu a}. \quad (24)$$

3. Uncertainty propagation for D'Agostini

One recent MicroBooNE cross-section analysis [87] used D'Agostini unfolding together with analytic propagation of uncertainties according to the prescription above. In this case, the unfolding matrix depends on the measured event counts when multiple iterations i are used, and the expression for the error propagation matrix becomes [88, 89]

$$\mathfrak{E}_{\mu a}^{i+1} = \frac{\partial \hat{\phi}_{\mu}^{i+1}}{\partial d_a} = U_{\mu a}^i + \frac{\hat{\phi}_{\mu}^{i+1}}{\hat{\phi}_{\mu}^i} \mathfrak{E}_{\mu a}^i - \sum_{\lambda,b} \epsilon_{\lambda} \frac{d_b}{\hat{\phi}_{\lambda}^i} U_{\mu b}^i U_{\lambda b}^i \mathfrak{E}_{\lambda a}^i. \quad (25)$$

with $\mathfrak{E}_{\mu a}^0 = 0$. The covariance matrix describing the uncertainty on the unfolded event counts obtained from

the final iteration f is given by

$$\text{Cov}(\hat{\phi}_\mu^f, \hat{\phi}_\lambda^f) = \sum_{a,b} \mathfrak{E}_{\mu a}^f \text{Cov}(d_a, d_b) \mathfrak{E}_{\lambda b}^f. \quad (26)$$

4. Reference-flux measurement

In contrast to MINERvA-style cross-section extraction, the MicroBooNE approach produces a measurement in the *reference* flux estimated from the nominal simulation. This is a consequence of the choice to directly vary the expected event counts n_a in the flux systematic universes rather than using the prescription from Eq. 18 in which signal events are only adjusted through variations in the detector response matrix $\Delta_{\mu a}$. A key assumption in this choice is that the neutrino energy dependence of the total cross section $\sigma(E_\nu)$ from the nominal simulation is sufficiently realistic to be used to propagate beam flux uncertainties into the expected event counts n_a .

This also leads to a subtle change in the interpretation of the measured event counts D_a . These are observed numbers of events measured in the real flux, and they are interpreted as such under a MINERvA-like approach. However, the MicroBooNE uncertainty prescription treats them as estimators of the event counts that *would have* been measured in the reference flux. Since the reference flux used is the best available estimate of the real flux, no correction is needed to the values of the D_a in the analysis.

Because the full effect of the flux and target-counting systematic variations is already included in the pre-unfolding covariance matrix, the denominator in Eq. 20 uses the central-value estimates of Φ and T without assigning any additional uncertainty.

5. Use of the regularization matrix

To account for the bias introduced by unfolding methods that use regularization, occasionally an ad hoc systematic uncertainty is added to an analysis. For example, because the D'Agostini method approaches direct inversion in the limit of many iterations, an implicit regularization is applied by the choice of the total iteration count f . Some neutrino cross-section analyses have therefore taken the spread between the results obtained with different numbers of iterations as an additional uncertainty on the unfolding procedure itself [60, 64, 65].

Although well-intended, application of this extra uncertainty decreases the statistical power of the measurement unnecessarily. The authors of Ref. [82] recommend instead that the regularization matrix A_C be reported together with the unfolded cross-section results. If one multiplies a theoretical prediction in the true bins by A_C before a goodness-of-fit metric is calculated, then the regularization is applied to the prediction and the data in a

consistent way, avoiding the need for any additional uncertainty. The degree to which A_C differs from the identity matrix also provides a convenient way of quantifying the level of bias introduced by the chosen regularization.

All MicroBooNE cross-section publications to date that have used Wiener-SVD unfolding have followed this approach [76–81]. However, the calculation of A_C is simple for any unfolding method expressible as a linear transformation of the data. For an arbitrary unfolding matrix U , it follows immediately from the definitions in Eqs. 14 and 15 that

$$A_C = U \cdot \Delta. \quad (27)$$

For MINERvA-like uncertainty treatments in which the unfolding matrix is recalculated in each systematic universe, the central-value version should be used to obtain A_C for use in a data release.

C. T2K-style extraction

Like MicroBooNE, the T2K collaboration has developed a unique cross-section extraction procedure that has become the preferred method in their recent analyses [90–97]. In two early publications [52, 55], the new T2K technique was used to report some results while others were obtained using a MINERvA-style approach.

The core of the T2K strategy is a binned likelihood fit to the data involving a large number of parameters. This fit is used for unfolding, background removal, and at least the first stage of uncertainty quantification. The Minuit2 code [98], a C++ translation of the Fortran software package MINUIT [99], provides the algorithms used for numerical optimization. An initial implementation of the T2K fitting framework is publicly available in the form of the xsLLhFitter [100] code. However, further software development effort appears to be focused instead on a forked version called GUNDAM [101].

1. Binned likelihood fit

For the T2K fitting framework, the task of interest is minimization of minus two times the logarithm of the likelihood function:

$$-2 \log(\mathcal{L}) = -2 \log(\mathcal{L}_{\text{stat}}) - 2 \log(\mathcal{L}_{\text{syst}}) - 2 \log(\mathcal{L}_{\text{reg}}). \quad (28)$$

This quantity is identical to the chi-squared statistic (χ^2) when all parameters of interest follow a multivariate Gaussian distribution. This is true for the $\mathcal{L}_{\text{syst}}$ term but not the others.

a. Statistical term The statistical contribution to the log-likelihood may be written as

$$-2 \log(\mathcal{L}_{\text{stat}}) = 2 \sum_a \mathcal{P}_a, \quad (29)$$

where the sum runs over all reconstructed bins a . In the earliest versions of the T2K fitter, \mathcal{P}_a took the simple form [55]

$$\mathcal{P}_a = n_a - D_a + D_a \log\left(\frac{D_a}{n_a}\right) \quad (30)$$

where D_a (n_a) is the measured (predicted) number of events in the a -th reconstructed bin. This expression is the negative log-likelihood for a Poisson distribution after applying Stirling's approximation [102]

$$\log(D_a!) \approx D_a \log(D_a) - D_a. \quad (31)$$

More recent updates to the T2K fitter described in Refs. [91, 92] have added corrections to the Poissonian likelihood for finite Monte Carlo (MC) statistics in the calculation of the n_a using the Barlow-Beeston approach [103, 104]. This yields a new expression

$$\mathcal{P}_a = \beta_a n_a - D_a + D_a \log\left(\frac{D_a}{\beta_a n_a}\right) + \frac{\beta_a^2 - 1}{2\sigma_a^2} \quad (32)$$

where σ_a^2 is the relative MC statistical variance of n_a and

$$\beta_a = \frac{1}{2} \left[1 - n_a \sigma_a^2 + \sqrt{(n_a \sigma_a^2 - 1)^2 + 4 D_a \sigma_a^2} \right]. \quad (33)$$

In the limit of infinite simulated events, the expression in Eq. 30 is recovered via $\sigma_a^2 \rightarrow 0$.

b. Systematic term The systematic contribution in Eq. 28 takes the form

$$-2 \log(\mathcal{L}_{\text{syst}}) = (\mathbf{p} - \mathbf{p}^{\text{CV}})^T \cdot V_{\text{syst}}^{-1} \cdot (\mathbf{p} - \mathbf{p}^{\text{CV}}) \quad (34)$$

and acts as a Gaussian penalty term that prevents the systematic parameters \mathbf{p} varied in the fit from deviating implausibly far from their fixed central values \mathbf{p}^{CV} . The covariance matrix V_{syst} describes the prior uncertainties on the systematic parameters, including their correlations.

The predicted events n_a in each reconstructed bin are calculated as a function of the systematic parameters via

$$n_a = \sum_{\mu} [c_{\mu} \phi_{\mu a}(\mathbf{p}) + B_{\mu a}(\mathbf{p})] \quad (35)$$

where $\phi_{\mu a}$ ($B_{\mu a}$) is the simulated number of signal (background) events that fall simultaneously into the μ -th true bin and the a -th reconstructed bin. An additional parameter c_{μ} is included in the fit for each true bin μ . Since the c_{μ} are unconstrained by the systematic log-likelihood in Eq. 34, the signal prediction is allowed to float in the fit to match the data.

Due to the large computational cost of running the simulation repeatedly, the dependence of the signal ($\phi_{\mu a}$) and background ($B_{\mu a}$) predictions on the systematic parameters \mathbf{p} is evaluated via reweighting. Under this approach, a large set of MC events is first generated using

the nominal simulation. To obtain a prediction for an alternative simulation ($\mathbf{p} \neq \mathbf{p}^{\text{CV}}$), a statistical weight is assigned to each event based on its relative likelihood of occurring in the systematic universe of interest.

c. Regularization term Minimization of the log-likelihood formed by the first two terms from Eq. 28 is similar to directly inverting the detector response matrix (see Sec. II B 1) and gives an equivalent result under certain conditions [52, Sec. IV D 1]. While the best-fit values of the parameters c_{μ} and \mathbf{p} are obtained with minimal bias, the procedure suffers from the same difficulties as direct inversion. In particular, the fit tends to be highly sensitive to small statistical fluctuations in the measured event counts D_a and to yield a corresponding estimator of the observed signal event counts with strong negative correlations between neighboring bins.

Similarly to the D'Agostini and Wiener-SVD unfolding strategies, which address these concerns by modifying direct matrix inversion using prior information about the expected result, regularization can also be applied in the T2K fitting technique. In this case, the prior information is represented by an optional third term in the log-likelihood function. The form of this third term is ultimately arbitrary and may be defined in an analysis-specific way. However, a choice used in multiple T2K publications [52, 93, 96] is a version of Tikhonov-Phillips regularization [105, 106] in which a smoothness condition is imposed on the signal scaling parameters c_{μ} via

$$-2 \log(\mathcal{L}_{\text{reg}}) = \tau_{\text{reg}} \sum_{\mu} (c_{\mu+1} - c_{\mu})^2. \quad (36)$$

Here the sum runs over pairs of neighboring true bins μ and $\mu + 1$ representing the same observable. The quantity in parentheses is proportional to the first derivative of the c_{μ} under a forward difference approximation.

The regularization strength τ_{reg} is a constant that controls the relative importance of this term in the likelihood fit. In the T2K analyses adopting regularization of this kind, the value of τ_{reg} was chosen using an *L-curve* technique [107]. This approach seeks an optimal regularization strength by repeating the fit many times for different τ_{reg} values. Each fit result contributes a point to a parametric curve in which the x and y coordinates are given by

$$\mathcal{X} = -2 \log(\mathcal{L}_{\text{stat}}) - 2 \log(\mathcal{L}_{\text{syst}}), \quad (37)$$

and

$$\mathcal{Y} = \frac{-2 \log(\mathcal{L}_{\text{reg}})}{\tau_{\text{reg}}}. \quad (38)$$

Both coordinates are evaluated after minimizing the full log-likelihood $-2 \log(\mathcal{L})$ at fixed τ_{reg} . Because \mathcal{X} tends to increase and \mathcal{Y} tends to decrease as the regularization strength grows, the parametric curve $(\mathcal{X}, \mathcal{Y})$ is expected to have a characteristic *L* shape. Choosing the τ_{reg} value corresponding to the point of maximum curvature (i.e.,

the kink in the L) thus represents an optimal balance between compatibility with the regularization criterion (minimal \mathcal{Y}) and compatibility with the measured data (minimal \mathcal{X}).

d. Fit results To minimize the log-likelihood function defined in Eq. 28, the T2K fitter uses the MIGRAD algorithm [90, 99] as implemented in Minuit2. The unfolded signal event counts $\hat{\phi}_\mu$ in each true bin μ are then calculated after minimization via

$$\hat{\phi}_\mu = \frac{1}{\epsilon_\mu} \sum_a c_\mu^{\text{PF}} \phi_{\mu a}(\mathbf{p}^{\text{PF}}), \quad (39)$$

where the sum includes all relevant reconstructed bins a .

This leads to the measured differential cross section

$$s_\mu = \frac{\hat{\phi}_\mu}{\Phi T \Delta \mathbf{x}_\mu}. \quad (40)$$

where the abbreviation defined in Eq. 12 is used once again. The superscript PF that appears in Eq. 39 denotes the post-fit values of the parameters. The efficiency ϵ_μ , integrated flux Φ , and number of scattering targets T are also evaluated using the post-fit parameters. For example, the efficiency can be estimated from the T2K simulation as

$$\epsilon_\mu = \frac{\sum_a \phi_{\mu a}(\mathbf{p}^{\text{PF}})}{\phi_\mu(\mathbf{p}^{\text{PF}})} \quad (41)$$

where ϕ_μ is the total number of simulated signal events in the μ -th true bin.

2. Fit parameter covariances

In addition to providing a means of extracting the measured differential cross sections s_μ , the log-likelihood function from Eq. 28 encodes detailed information about the relationships between all parameters included in the fit. Using the HESSE algorithm [90, 99] from Minuit2, an approximate covariance matrix describing uncertainties on the fit parameters may be obtained by calculating the elements of the *Hessian matrix*

$$H_{\text{qb}} = -\frac{\partial^2 \log(\mathcal{L})}{\partial K_{\text{q}} \partial K_{\text{b}}} \Big|_{\mathbf{K}=\mathbf{K}^{\text{PF}}} \quad (42)$$

and then inverting it:

$$\text{Cov}(K_{\text{q}}, K_{\text{b}}) \approx (H^{-1})_{\text{qb}}. \quad (43)$$

Here the signal scaling factors c_μ and the systematic parameters included in \mathbf{p} all appear as individual elements

K_{q} of a combined vector of fit parameters

$$\mathbf{K} = \begin{pmatrix} c_0 \\ c_1 \\ \vdots \\ \mathbf{p} \end{pmatrix}. \quad (44)$$

Cyrillic subscripts (ч , ъ) are used as parameter indices to avoid confusion with those used to identify the true and reconstructed bins. The post-fit values \mathbf{K}^{PF} define the point in parameter space where the Hessian matrix elements H_{qb} are evaluated. The approximate equality in Eq. 43 becomes exact when all of the K_{q} follow a multivariate Gaussian distribution [108] and when the second partial derivatives in Eq. 42 are exactly calculable.

3. Uncertainty propagation

Two distinct strategies have been used in T2K analyses for assigning an uncertainty to the differential cross sections s_μ measured using a binned likelihood fit.

In Ref. [93, Sec. IV E 1], a MINERvA-like multiple-universe extraction approach (see Sec. II A 2 herein) is adopted. In this case, a single set of universes is generated by varying all systematic parameters simultaneously, and the fitting procedure is repeated in each universe u to yield a new measurement s_μ^u . The arithmetic mean of the results \bar{s}_μ is taken to be the final measured cross section, and the covariance matrix describing its uncertainty is calculated according to Eq. 11. Statistical uncertainties are included in the multiple-universe treatment by fluctuating the contents of the reconstructed bins according to a Poisson distribution.

In Refs. [91, 92], repetition of the likelihood fit is avoided by use of the parameter covariance matrix mentioned above. Each of the N_{univ} universes is now generated by sampling a set of parameter values \mathbf{K}^u from the multivariate Gaussian distribution with mean \mathbf{K}^{PF} and covariance matrix $\text{Cov}(K_{\text{q}}, K_{\text{b}})$. The final measured cross section is taken to be the value calculated with the post-fit parameters $s_\mu^{\text{PF}} \equiv s_\mu(\mathbf{K}^{\text{PF}})$, and the elements of the corresponding covariance matrix are obtained via

$$\text{Cov}(s_\mu, s_\lambda) = \frac{1}{N_{\text{univ}}} \sum_{u=1}^{N_{\text{univ}}} (s_\mu^u - s_\mu^{\text{PF}})(s_\lambda^u - s_\lambda^{\text{PF}}), \quad (45)$$

where $s_\mu^u = s_\mu(\mathbf{K}^u)$ is the differential cross section evaluated in the u -th universe. Note that the values of ϵ_μ , Φ , and T are updated in each universe to be consistent with the other parts of the calculation in Eqs. 39 and 40.

4. Flux treatment

The standard T2K method for cross-section extraction produces a real-flux result with the same require-

ments for properly treating the flux shape uncertainty as MINERvA's measurements (see Sec. II A 3). However, one recent T2K analysis [90] reported a reference-flux cross section instead by applying an extrapolation discussed in Ref. [46], which I summarize here.

Without loss of generality, arrange the elements of the vector of systematic parameters \mathbf{p} so that

$$\mathbf{p} = \begin{pmatrix} \boldsymbol{\psi} \\ \boldsymbol{\theta} \end{pmatrix}, \quad (46)$$

where the vector $\boldsymbol{\psi}$ contains the subset of parameters that affect the neutrino flux model, while $\boldsymbol{\theta}$ contains those that do not. To extract a cross-section measurement in a specific reference flux, the binned likelihood fit and, if needed, the parameter covariance calculation from Eq. 43 are carried out unaltered. However, when evaluating the differential cross section in a systematic universe (s_μ^u) or at the post-fit point (s_μ^{PF}), the values of the flux parameters $\boldsymbol{\psi}$ that would normally be used are ignored and replaced with constants corresponding to the reference flux: $\boldsymbol{\psi} \rightarrow \boldsymbol{\psi}^{\text{ref}}$. This replacement applies to all component parts of the cross-section calculation, including ϵ_μ and Φ . Thus, as is the case for the MicroBooNE extraction procedure (see Sec. II B 4), the measurement becomes an estimator for the cross section that *would have been* observed in the reference flux.

III. BLOCKWISE UNFOLDING

In recent years, there has been growing recognition of the importance of correlated uncertainties in the interpretation of neutrino cross-section data, particularly for quantitative comparisons and model parameter tuning. While early cross-section results from MiniBooNE established many analysis techniques that remain influential for modern experiments, a notable but not universal [58, 59, 61] omission in some of the collaboration's data releases [109] is the lack of a full covariance matrix describing bin-to-bin correlations in the measurement uncertainties [60, 62–64]. Such correlations arise from both systematic and statistical effects, the latter as a result of unfolding even when the reconstructed bins are disjoint. Difficulties created by the missing MiniBooNE correlations in assessing agreement of predictions with the data [74, 110] and in fitting model parameters [111, 112] led to widespread consensus on the need for this information and multiple calls for its inclusion in future results [4, 113]. Problems with missing correlations of this kind are not limited to neutrino data sets; efforts to constrain uncertainties on intranuclear cascade models using hadron-nucleus data have also had to confront them [114].

Happily, data reporting strategies in the field were quick to adapt in light of these limitations, and presenting a flux-averaged differential cross section together with a corresponding uncertainty covariance matrix is now stan-

dard practice. Although the value of this step forward should not be understated, a primary goal of the present work is to recommend and enable the inclusion of still more detailed information about measurement correlations in cross-section data releases by neutrino experiments.

A. Missing correlations

Specifically, there are two types of covariances that are usually not reported but nevertheless highly valuable for data interpretation. The first type arises for measurements in which multiple kinematic distributions are presented, typically using a consistent signal definition, event selection, and data set in the analysis. A recent example is Refs. [78, 79] from MicroBooNE, in which various one- and two-dimensional differential cross sections are measured using a single set of 9051 quasielastic-like event candidates. Each differential cross section reported therein thus represents a particular projection of a higher-dimensional joint distribution describing the relationship between all relevant kinematic variables. In the absence of a measurement of the full joint distribution, the most stringent test of an interaction model is obtained by requiring it to describe all of the low-dimensional projections simultaneously. However, inter-projection covariances, i.e., those correlating a bin from one measured differential cross section with a bin from another, are rarely provided in the literature. This presents a major problem when attempting to quantify overall goodness-of-fit between a model prediction and a multi-projection data set; strong inter-distribution correlations are expected from both systematic uncertainties (e.g., beam flux modeling) and statistical fluctuations (shared events).

A second type of covariance that is typically unavailable is evaluated between cross-section results obtained by distinct analyses from the same experiment. Many of the motivations and challenges for reporting this information are shared with the first type, but there are additional practical concerns, such as a possibly long time delay between execution of the two measurements. Careful planning to ensure that inter-analysis covariances can be evaluated, however, would do much to overcome difficulties encountered by multiple groups examining neutrino scattering data over the past decade. In Refs. [111] and [115], for example, presumably strong correlations between neutrino and antineutrino cross sections measured separately by the same experiment had to be neglected due to the lack of a suitable data release.²

Missing covariances of both types posed a challenge for a model fitting study [116] in which the MINERvA

² Note, however, that the T2K data studied in Ref. [115] included such correlations while the MINERvA data did not.

collaboration tuned parameters in the GENIE event generator [117, 118] to four of their published pion production cross-section measurements [25, 28, 36]. Inter-distribution correlations (first type) were handled with an ad hoc approach to calculating the χ^2 statistic, while inter-analysis correlations (second type) were neglected entirely. The authors are forthright in the paper about the limitations of these approximations, which were adopted despite unfettered access to MINERvA’s data and analysis tools. This suggests that, even when an experiment has dedicated substantial effort to data preservation [119], retroactively obtaining correlations between existing analyses may be prohibitively difficult in many cases.

B. Precedents

Since retrofitting existing results with more detailed uncertainty quantification may not be feasible, one may instead design future neutrino cross-section analyses in a way that facilitates reporting complete covariances of both types. In the remainder of this section, I describe a mathematical procedure intended to accomplish this goal.

Some elements of this procedure appear to have already been applied in recent T2K analyses that made simultaneous measurements of neutrino and antineutrino cross sections [95] and neutrino cross sections on both carbon and oxygen targets [93]. However, in that context, the primary motivation was robust separation of signal and background, and the presentation is entirely specific to a T2K-style cross-section extraction. Several MINERvA publications have also reported simultaneous measurements of neutrino cross sections on multiple targets [8, 11, 26]. Although these publications report uncertainty covariance matrices only for each individual distribution and its ratio to the corresponding distribution for hydrocarbon, a proper handling of the uncertainties for the latter suggests that a full set of covariances between hydrocarbon and the other targets must have been obtained at some stage of the analysis. Since the uncertainty treatment is not described in detail, however, it is difficult to generalize to other applications.

With the aim of encouraging experimental collaborations to further strengthen their neutrino cross-section data releases, I build upon these precedents to develop a general recipe called *blockwise unfolding* for evaluating covariances between distinct flux-averaged differential cross section measurements. I also discuss this method’s possible application to evaluating covariances between results obtained by separate analyses from the same experiment. This includes identifying the specific information that must be preserved to avoid time-consuming repetition of an earlier analysis for this purpose.

The blockwise unfolding technique is compatible with at least some versions of all three cross-section extraction strategies reviewed in Sec. II. Since incorporating block-

wise unfolding within a MicroBooNE-style measurement is the case that requires the most detailed explanation, I assume it for an initial presentation below. Adjustments appropriate for MINERvA- and T2K-style cross-section extraction are then considered as an expansion of the prior material.

C. MicroBooNE-style measurements

As discussed in Sec. II B, MicroBooNE’s cross-section extraction method involves evaluating a complete set of uncertainties on the number of events measured in each reconstructed bin. A final result is obtained by applying consistent linear transformations to both the background-subtracted data and the total covariance matrix describing the reconstructed event counts. To generalize the procedure to allow reporting the covariances between bins in distinct kinematic distributions, two significant problems must be solved. First, the covariance matrix describing the statistical uncertainty on the measured event counts must be constructed in a way that respects the correlations that arise due to events that are shared between distributions. Second, the linear transformation applied to the data, which amounts to unfolding and division by a few constant scaling factors, must be performed in a way that preserves the inter-distribution covariances evaluated between reconstructed bins.

1. Statistical correlations

In the traditional case where neutrino cross sections are reported individually for each kinematic distribution, calculation of the statistical covariance matrix is simple. Each measured event belongs to exactly one reconstructed bin, and hence the individual bin contents before unfolding follow independent Poisson distributions. The statistical covariance matrix is diagonal, and the number of observed counts D_a in the a -th reconstructed bin is an estimator of its variance.

When multiple distributions are extracted simultaneously from the same data set, events can be shared between bins, and the assumption of independent Poisson fluctuations in each bin is no longer valid. However, a general expression for an estimator of the statistical covariance between an arbitrary pair of kinematic bins, which I will label X and Y , is easy to derive when the problem is framed suitably.

As illustrated in Fig. 1, the key trick is to subdivide bins X and Y into three non-overlapping bins u , v , and w . Bin v is defined to contain only those events that belong simultaneously to bins X and Y , while bin u (w) contains the events that belong solely to bin X (Y). By definition, then, bins u , v , and w have no events in common, and the measured event counts in each follow independent Poisson distributions. It follows from the descriptions

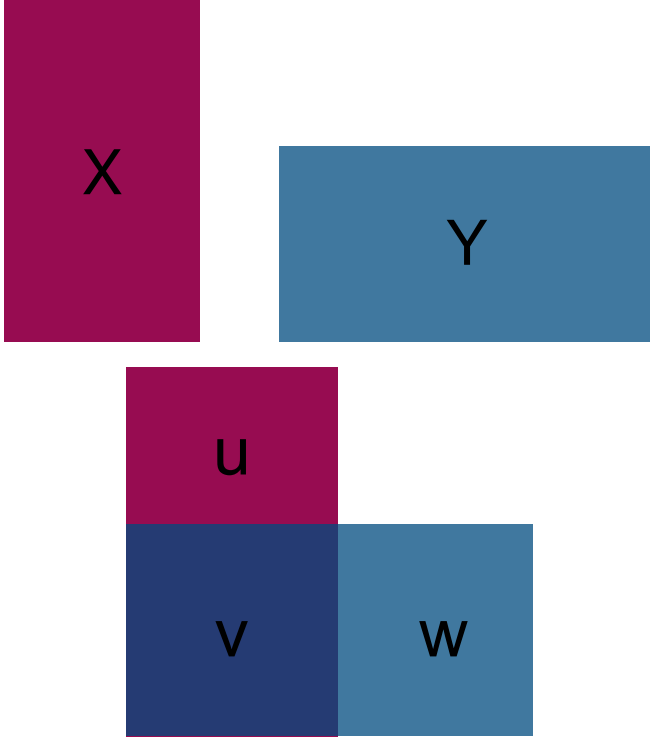


Figure 1: A pair of arbitrary kinematic bins X and Y (top) can always be subdivided into three non-overlapping bins u , v , and w (bottom). This observation allows a straightforward derivation of the statistical covariance between bins X and Y .

above that the covariance between the measured event counts in bin X and bin Y is given by

$$\begin{aligned} \text{Cov}(D_X, D_Y) &= \text{Cov}(D_u + D_v, D_v + D_w) \\ &= \text{Cov}(D_u, D_v) + \text{Cov}(D_u, D_w) \\ &\quad + \text{Cov}(D_v, D_w) + \text{Cov}(D_v, D_v) \\ &= 0 + 0 + 0 + \text{Var}(D_v) \approx D_v. \end{aligned} \quad (47)$$

In the last approximate equality, the measured number of events D_v in bin v is used as an estimator of its variance. Thus, the statistical covariance between any two reconstructed bins can be estimated simply by calculating the number of events that they have in common. This result becomes particularly intuitive in the limits where X and Y are identical and where they are disjoint.

The same derivation can also be applied to evaluate Monte Carlo statistical uncertainties on a simulation prediction. In the case of weighted events, which are used to adjust a nominal simulation by the NOvA [120] and MicroBooNE [86] collaborations among others, the appropriate estimator for the variance of bin v is the sum of the squared weights of the events that it contains. In the limit of unit weights for all events, this reduces to the simple event count appropriate for measured data and an unweighted MC prediction.

2. Unfolding complete covariances

Unlike the statistical covariances, evaluation of the systematic covariances between bins from different kinematic distributions proceeds without any subtleties. For the case of a MicroBooNE-style analysis, the formula from Eq. 17 can be used unaltered for all pairs of reconstructed bins a and b to be included in the final measurement. To avoid double-counting, however, the sum over μ in Eq. 18 should include only the true bins belonging to the same block (defined below) as reconstructed bin a .

To simplify propagation of the results through unfolding, I recommend a specific scheme for organizing the analysis bins. Define the term *block* to refer to a group of related true and reconstructed bins intended for use in a measurement of the same distribution of observables \mathbf{x} . Apart from individual bin limits on the values of these observables, the same signal definition should be shared by all true bins belonging to the same block, and a single set of selection criteria should apply to all reconstructed bins in the block. Within a properly-formed block, there should also not be any phase-space gaps or bin overlaps; any simulated signal interaction that fulfills all relevant event selection criteria should belong to exactly one true bin and exactly one reconstructed bin within the block. Note that there is no requirement for distinct blocks to have the same signal definition, event selection criteria, or observables of interest \mathbf{x} . I will assume below, however, that all bins in the analysis of interest have been grouped into valid blocks.

To proceed with the remainder of MicroBooNE-style cross-section extraction, an unfolding matrix U_b should be constructed separately for each individual block b . There is no restriction on the specific recipe to be used for computing U_b , and a unique unfolding method can be used in each block if desired. The formulas for calculating the unfolding matrix, given in the preceding sections and in Appendix A, can still be used in this case as long as they are evaluated while ignoring all bins outside of the block of interest b . For example, the sums over true and reconstructed bins that appear in Eqs. 7, 9, and 10 for D'Agostini unfolding should include only bins belonging to the current block. When computing the per-block error propagation matrix \mathfrak{E}_b needed for MicroBooNE-style propagation of uncertainties (see Sec. II B 2), bins outside of block b should also be ignored in the same way.

The matrices for the individual blocks may be used to form an overall unfolding matrix U and an overall error propagation matrix \mathfrak{E} via direct sums:

$$U = \bigoplus_{b=0} U_b = U_0 \oplus U_1 \oplus \dots = \begin{pmatrix} U_0 & 0 & 0 & \dots \\ 0 & U_1 & 0 & \dots \\ 0 & 0 & \ddots & \dots \\ \vdots & \vdots & \vdots & \ddots \end{pmatrix}, \quad (48)$$

and

$$\mathfrak{E} = \bigoplus_{b=0} \mathfrak{E}_b. \quad (49)$$

These can then be used to extract final cross-section results involving all bins. Likewise, if one forms an overall detector response matrix from the response matrices calculated for individual blocks,

$$\Delta = \bigoplus_{b=0} \Delta_b, \quad (50)$$

then Eq. 27 can be used to compute the regularization matrix A_C describing the entire measurement.

In the most general case, bins belonging to different blocks may involve different observables, and different scaling factors may be appropriate for converting their unfolded contents to a differential cross section. I thus update the notation from prior sections to obtain the new formulas

$$\left\langle \frac{d^n \sigma}{d\mathbf{x}} \right\rangle_\mu = \frac{\hat{\phi}_\mu}{\Phi_\mu T_\mu \Delta\mathbf{x}_\mu} = \frac{\sum_a U_{\mu a} (D_a - B_a)}{\Phi_\mu T_\mu \Delta\mathbf{x}_\mu}, \quad (51)$$

and

$$\text{Cov} \left(\left\langle \frac{d^n \sigma}{d\mathbf{x}} \right\rangle_\mu, \left\langle \frac{d^n \sigma}{d\mathbf{y}} \right\rangle_\lambda \right) = \frac{\sum_{a,b} \mathfrak{E}_{\mu a} \text{Cov}(D_a, D_b) \mathfrak{E}_{\lambda b}}{\Phi_\mu \Phi_\lambda T_\mu T_\lambda \Delta\mathbf{x}_\mu \Delta\mathbf{y}_\lambda}. \quad (52)$$

Here n (m) is the number of observables \mathbf{x} (\mathbf{y}) for which a differential cross section is reported in true bin μ (λ), and $\Delta\mathbf{x}_\mu$ ($\Delta\mathbf{y}_\lambda$) is the corresponding product of bin widths.

True bin indices μ and λ appear above as subscripts on the integrated flux Φ and number of scattering targets T . In this context, they indicate that the value of Φ or T that should be used is the one for the block containing the true bin μ or λ . Differences in the signal definition between blocks may necessitate the use of distinct values in some cases, such as a discrepancy between the neutrino flavors of interest (Φ) or the fiducial volumes in which events are accepted (T) by the analysis. All other notation in these expressions is defined as in previous sections, and all bin indices may refer to an element of any block.

Because the overall unfolding and error propagation matrices from Eqs. 48–49 are block diagonal, the measured cross sections and covariances within block b are identical to the results that would have been obtained if a standalone measurement had been performed for block b alone using the unfolding matrix U_b and error propagation matrix \mathfrak{E}_b . However, since the reconstructed-space covariance matrix $\text{Cov}(D_a, D_b)$ includes complete inter-block correlations and is propagated through the extraction procedure, these correlations are appropriately preserved in the final result.

D. Simplifying data releases

When working with multiple blocks involving different observables ($\mathbf{x} \neq \mathbf{y}$ above), an unfortunate feature of the expression given in Eq. 52 is that the units needed to express the covariance matrix elements will vary with the true bin indices μ and λ . In particular, it is possible for the units of the off-diagonal elements of the covariance matrix connecting two separate blocks to differ from the units of the covariances contained within either block. Especially for an analysis involving many distinct blocks, expressing the measurement in this form is cumbersome and unnecessarily confusing.

To avoid this issue entirely, I recommend an alternative but entirely equivalent way of representing the data. Using the same notation as in Sec. I, define the flux-averaged total cross section in true bin μ by

$$\langle \sigma \rangle_\mu \equiv \int_{\mathbf{x}_\mu}^{\mathbf{x}_{\mu+1}} \left\langle \frac{d^n \sigma}{d\mathbf{x}} \right\rangle d\mathbf{x}. \quad (53)$$

As implied by Eq. 6, this quantity is just the product of the average differential cross section in the bin multiplied by the n bin widths:

$$\langle \sigma \rangle_\mu = \left\langle \frac{d^n \sigma}{d\mathbf{x}} \right\rangle_\mu \cdot \Delta\mathbf{x}_\mu. \quad (54)$$

It follows from this that Eqs. 51–52 may be rewritten in terms of the flux-averaged total cross sections as

$$\langle \sigma \rangle_\mu = \frac{\hat{\phi}_\mu}{\Phi_\mu T_\mu} = \frac{\sum_a U_{\mu a} (D_a - B_a)}{\Phi_\mu T_\mu}, \quad (55)$$

and

$$\text{Cov} \left(\langle \sigma \rangle_\mu, \langle \sigma \rangle_\lambda \right) = \frac{\sum_{a,b} \mathfrak{E}_{\mu a} \text{Cov}(D_a, D_b) \mathfrak{E}_{\lambda b}}{\Phi_\mu \Phi_\lambda T_\mu T_\lambda}. \quad (56)$$

Since the bin widths $\Delta\mathbf{x}_\mu$ and $\Delta\mathbf{y}_\lambda$ are exactly known by definition, conversion to this new representation is trivial. The absence of these widths in Eqs. 55–56 conveniently allows a single set of units to be used to report all of the measured $\langle \sigma \rangle_\mu$ values (e.g., cm^2) and their covariances (e.g., cm^4).

For future cross-section analyses adopting blockwise unfolding, I therefore recommend the following format for an associated data release. The measured flux-averaged total cross sections $\langle \sigma \rangle_\mu$ should be expressed as a column vector of values ordered by bin number μ and sharing the same units. The covariances from Eq. 56 should likewise be expressed in a single matrix whose rows and columns correspond to the bin indices μ and λ , respectively. Each element of the matrix should be expressed in units equal to the square of the units used to report $\langle \sigma \rangle_\mu$. If available, the regularization matrix A_C should also be included with the results using the same ordering of the bin indices. The elements of A_C are dimensionless.

A table listing the bin definitions and block boundaries in order of bin number should also be provided to allow for straightforward evaluation (by dividing by the appropriate bin widths) of differential cross sections.

In addition to reducing the potential for unit-related confusion, this data presentation strategy has an additional advantage. Since division by the bin widths is performed by downstream users of the data only when needed, underflow and overflow bins for which at least one of the widths is infinite can be reported alongside ordinary bins without any required changes. This avoids the need for the ad hoc treatments that are sometimes employed in the literature, e.g., including events belonging to underflow and overflow bins in their closest finite-width neighbors as in Refs. [78, 79, 81].

E. MINERvA-style measurements

For blockwise unfolding within MINERvA’s approach to cross-section extraction, the guidelines above for organizing and presenting a measurement may be applied largely unaltered. However, instead of building a reconstructed-space total covariance matrix $\text{Cov}(D_a, D_b)$ and transforming it with the error propagation matrix \mathbf{E} , uncertainties are now quantified by re-extracting the cross sections in multiple alternative universes as described in Sec. II A 2. For the statistical uncertainties, these may include bootstrapping-based universes in which the observed bin contents are resampled according to the appropriate underlying distribution.

Provided that the full multi-block unfolding matrix U from Eq. 48 is recomputed in each universe, the change in uncertainty quantification strategy presents no special difficulties for the systematic variations. However, bootstrapping to evaluate the statistical uncertainties raises a new challenge. For a MicroBooNE-like analysis, considering correlations between individual pairs of bins is sufficient to calculate statistical covariance matrix elements (see Sec. III C 1). Construction of universes for this purpose, on the other hand, requires statistical resampling that accounts for correlations between all of the bins simultaneously.

To explain how this may be accomplished, I will specialize to the case of data statistical uncertainties, i.e., those on the vector of measured event counts \mathbf{D} in each reconstructed bin. Under a bootstrapping approach, these uncertainties are propagated by re-extracting the cross section in alternative universes u in which the elements D_a of \mathbf{D} are resampled according to Poissonian statistics to create a new vector \mathbf{D}^u . All other quantities involved in cross-section extraction for these universes are evaluated according to the nominal simulation.

When events are shared between the reconstructed bins a , resampling the values of each of the D_a^u according to independent Poisson distributions will incorrectly neglect inter-bin statistical correlations. Like the simpler two-bin case considered in Sec. III C 1, a suitable choice

of rebinning enables a straightforward solution.

For a total of R reconstructed bins in \mathbf{D} (i.e., included in the measurement of interest), define an alternate set of $2^R - 1$ reconstructed bins that I will call the *bootstrapping basis*. The measured event counts expressed in this new basis are contained in the vector \mathbf{F} , which may be written in terms of smaller vectors as

$$\mathbf{F} = \begin{pmatrix} \mathbf{f}_1 \\ \mathbf{f}_2 \\ \vdots \\ \mathbf{f}_R \end{pmatrix}. \quad (57)$$

For $k \in \{1, 2, \dots, R\}$, the smaller vector \mathbf{f}_k has a total of

$${}^R C_k = \binom{R}{k} = \frac{R!}{k!(R-k)!} \quad (58)$$

elements, each corresponding to one of the unique combinations of k of the original bins from \mathbf{D} . For example, each new bin represented by \mathbf{f}_1 collects events that uniquely belong to a single reconstructed bin in \mathbf{D} , the bins represented by \mathbf{f}_2 do the same for events that uniquely belong to a specific pair of the original bins, and the single element of \mathbf{f}_R is the number of events that are shared by all of the original bins.

Since the definitions of all of the new bins in the bootstrapping basis are mutually exclusive, the elements of \mathbf{F} follow independent Poisson distributions. One may therefore form a new universe to evaluate statistical uncertainties by resampling the elements of \mathbf{F} and then summing over those needed to recalculate each element of \mathbf{D} . All statistical correlations between the original bins will be respected automatically by construction.

A similar approach can be employed for bootstrapping MC statistical uncertainties, but the distribution appropriate for resampling will be binomial, and all quantities derived from simulation must be updated within each universe before cross-section extraction.

F. T2K-style measurements

Thanks to the flexibility of the T2K collaboration’s likelihood fitting technique, extracting blockwise-unfolded cross sections under their approach is largely automatic once a suitable binning scheme has been defined. Either of the two strategies for uncertainty propagation described in Sec. II C 3 may be applied, but see Sec. III G 2 below for an important caveat. Statistical uncertainties can be handled by creating alternate universes using the bootstrapping basis described above.

G. Inter-analysis covariances

Blockwise unfolding is general enough to handle cases in which measurements in distinct blocks are obtained

from different analyses of data from the same experiment. Nevertheless, evaluating correlated uncertainties between cross-section results produced asynchronously raises practical difficulties related to data preservation. To alleviate these difficulties, I consider below the minimal information that must be available in order to calculate inter-analysis covariances.

1. Event lists

Similar to blockwise unfolding within a single analysis, the major challenge for computing statistical covariance matrix elements between separate analyses is the need to treat the correlations arising from shared events. As discussed previously in Secs. III C 1 and III E, properly doing so requires knowledge of the overlaps between the contents of all reconstructed bins from all analyses of interest. In general, this is only feasible by tracking the reconstructed bin contents on an event-by-event basis.

The bookkeeping required for this task is ponderous but uncomplicated to implement if it is prepared in advance. First, a unique identifier needs to be assigned to each data and MC event considered in any of the relevant analyses. Experimental collaborations typically do this as a matter of course.³ Second, an event list must be prepared for each analysis. Each entry in the list must specify a unique event identifier together with an array of zero or more indices that represent the reconstructed bins to which the event belongs. In the case of weighted MC events, the statistical weights should also be included in each list entry if they are not otherwise easily accessible.

2. Universes

For systematic uncertainty quantification, the main requirement is access to the full sets of alternative universes adopted by each of the analyses. Situations in which these sets are inconsistent, such as when a collaboration's approach to estimating specific systematic uncertainties has changed over time, must necessarily be handled on a case-by-case basis. I will therefore assume full consistency here while recognizing that careful work may be needed to relate different descriptions of the same systematic effect across analyses.

For MicroBooNE-style measurements, the most convenient representation of the u -th systematic universe is the vector \mathbf{n}^u , whose elements are the expected total event counts n_a^u in each reconstructed bin a . The \mathbf{n}^u from each analysis can be used to construct an overall reconstructed-space covariance matrix according to Eq. 17.

³ An example identification scheme is the set of run, subrun, and event indices used within the art event-processing framework [121] adopted by multiple Fermilab experiments.

For MINERvA-style measurements, the universes are represented directly as alternative values of the unfolded measurement s_μ^u in each true bin μ . In this form, they can easily be re-used to compute inter-analysis covariances according to Eq. 11.

For T2K-style measurements, calculation of inter-analysis systematic covariances is only well-defined under the first of the two uncertainty propagation strategies described in Sec. II C 3. Under that approach, there is a one-to-one correspondence between each alternative universe and the extracted cross sections s_μ^u obtained in its individual likelihood fit. This allows the same universe definition u to be used across all analyses when computing covariances via Eq. 11. When the universes are instead constructed under the second approach, i.e., based upon the post-fit parameter covariance matrix $\text{Cov}(K_u, K_b)$ from Eqs. 42–43, this is no longer practicable. Separate analyses will, in general, have different post-fit parameter values \mathbf{K}^{PF} and covariances. Relating the distinct sets of universes generated from these different inputs may not be achievable in any rigorous way.

3. Calculating the covariances

With the event lists and universes in hand, there are two main recipes that can be used to obtain the final inter-analysis uncertainties. When all measurements of interest were performed in the MicroBooNE style, one may calculate both systematic and statistical contributions to the multi-analysis total covariance matrix in reconstructed space according to the prescriptions from Secs. II B 2 and III C 1. Using the overall error propagation matrix \mathfrak{E} from Eq. 49, the covariances between the final cross-section results can then be evaluated according to Eq. 52. Central values should be used for all of the scaling factors (e.g., Φ_μ) that appear therein.

In the more general case where at least one analysis was performed using a different cross-section extraction approach, a separate step is needed for the statistical uncertainties. These must be handled by preparing alternate universes using a bootstrapping basis (see Sec. III E) that considers the full set of R reconstructed bins from all of the measurements. The cross sections should then be re-extracted in each of these universes to propagate the uncertainties. In the re-extractions, central values should be assumed for all quantities not subject to the relevant kind of statistical fluctuation (data, MC). The results of this first step may be combined with the systematic universes, which are evaluated on the unfolded measurements via Eq. 11, to obtain a total inter-analysis covariance matrix.

When MicroBooNE-style measurements are included in this calculation, one must transform the expected event counts n_a^u used to represent each systematic universe u into a corresponding unfolded differential cross section s_μ^u . Fortunately, Eq. 52 implies that this amounts

to the simple expression

$$s_\mu^u = \frac{1}{\Phi_\mu T_\mu \Delta \mathbf{x}_\mu} \sum_a \mathfrak{E}_{\mu a} n_a^u. \quad (59)$$

IV. CONDITIONAL COVARIANCE BACKGROUND CONSTRAINT

Scientific interest in neutrino cross-section measurements is primarily driven by the need to refine nuclear interaction simulations⁴ and their underlying theoretical ingredients. Because these simulations play an essential role in the design and execution of the measurements themselves, great care must be taken to avoid biasing results toward the interaction model used to obtain them. In appreciation of the challenges posed by this potential bias, experimental collaborations invest considerable effort toward quantifying relevant systematic uncertainties, and best practices for minimizing model dependence in cross-section analyses are a subject of ongoing discussion [5, 74, 110, 132].

Regardless of the specific methods employed in any given analysis, neutrino cross-section extraction inherently relies upon simulation predictions in ways that make interaction model deficiencies a significant concern. While a thoughtful choice of the signal definition, measurement observables, and binning scheme for an analysis can help to prevent problematic unfolding [74], mock-data studies in which a cross section is extracted from an alternative simulation are also routinely used to detect and diagnose bias. In analyses for which the expected background rate remains appreciable after all event selection criteria have been applied, robust estimation of the residual contamination becomes important. For some classes of background, notably cosmic-ray and radiological activity, this can often be done by means of a direct measurement performed when the neutrino beam is not active. However, background mismodeling presents a hazard in the frequent cases where a simulation prediction must be used.

Although details of procedures for revealing and remedying inaccurate background estimates are often highly analysis-specific, an overall strategy is widely adopted in the neutrino scattering literature. As a supplement to the binning scheme used to extract the final cross-section results, one or more sets of additional reconstructed bins, which are referred to as *control samples* or *sidebands* [5], are defined with alternative selection criteria intended to enhance the contribution of background events. To provide the best possible constraints on the background prediction in the *signal region* (i.e., the original bins), the

sidebands are typically designed to cover a similar range of kinematic phase space and involve minimal changes to the event selection. Good agreement between measured and predicted event counts in the sideband bins is interpreted as evidence that the simulation is reliable enough to use for background subtraction. When significant discrepancies are found, corrective adjustments can be applied to the simulation in various ways.

A. Use of sideband constraints by experiments

A methodological strength of the T2K fitting technique for cross-section extraction (Sec. II C) is that sideband-based background constraints can be incorporated simply by including the new bins in the likelihood fit. Correlations between the sideband bins and those used in the final measurement will automatically be described according to the experiment's full simulation of beam production, interaction physics, and the detector response.

Many MINERVA cross-section analyses [6, 7, 10, 11, 17, 18, 20, 21, 24, 26, 29, 30, 32] share a general approach to the use of sidebands that has also been employed in a few measurements by T2K [50, 53, 54] while extracting cross sections in the MINERVA style (Sec. II A). To apply this method, one may re-express the background prediction B_a in the a -th reconstructed bin (see Eq. 3) as

$$B_a = \sum_b \alpha_b B_{ab} \quad (60)$$

where the varieties of background are indexed by the Icelandic letter thorn (\flat) and B_{ab} is the expected number of background events of type \flat in the a -th reconstructed bin. Prior to inspection of the sideband data, the scale factors α_b are all set to unity, and B_a thus takes a value unaltered from the nominal simulation.

By fitting the normalization of the predicted background components \flat to the data in the sideband bins, updated values of the scale factors are obtained. Specifics of the fitting procedure are not always exhaustively documented and can differ substantially between analyses, including whether the signal prediction is also allowed to vary in the fit, whether multiple sidebands are fit separately or simultaneously, and whether the bins that will be used for the final measurement are fit together with the sidebands. Ultimately, the updated scale factor α_b is assigned a value based upon the ratio of the post-fit and pre-fit predictions of the number of background events of type \flat in the relevant sideband(s). The updated scale factors are then applied in Eq. 60 to compute the values of B_a actually used in cross-section extraction.⁵

⁴ Established neutrino scattering simulation codes for GeV energies include GENIE [117, 118], GiBUU [122–124], NEUT [125, 126], and NuWro [127–129], while ACHILLES [130, 131] is an emerging effort.

⁵ In some analyses, the scale factors are evaluated separately in different kinematic regions. This can be handled in the formal-

Although rarely described explicitly [30, 54], the standard method of incorporating this background modeling constraint into a MINERvA-style uncertainty treatment appears to be repeating the sideband fits during cross-section re-extraction in each systematic universe (Sec. II A 2). The statistical uncertainty on the fit results may be addressed by adding new universes in which the scale factors themselves are varied appropriately.

While comparatively simple to incorporate into a cross-section analysis, the most straightforward implementation of the MINERvA background constraint strategy has some limitations relative to the T2K likelihood fit. First, since the MINERvA method adjusts only normalization scale factors, sideband constraints are by construction unable to influence the shape of the individual classes of background to be subtracted. Second, in cases where the original bins to be used for the cross-section measurement are not included in the scale factor fit, a 100% correlation is implicitly assumed to exist between the background normalization in the sidebands and in the signal region. Obvious problems arising from these limitations can be detected by examining the level of agreement between the constrained simulation and data. If necessary, modifications can be made to improve the agreement, such as assigning separate scale factors in different kinematic ranges.

In contrast to T2K and MINERvA, MicroBooNE has not reported the use of control samples to validate the background model or apply a data-driven constraint for any of their differential cross section measurements released so far [65, 71–73, 76–81, 87]. The predicted background from simulation is simply used as-is without any analysis-specific changes to the central value or the modeling uncertainties. Such an approach has occasionally also been used by MINERvA [14–16], but only in cases where the expected background is very small.

A possible reason for the omission of sidebands in many of these analyses by MicroBooNE is that it may not necessarily be obvious how to incorporate a background model constraint into the systematics treatment needed to apply the Wiener-SVD unfolding method (Sec. II B 2). However, multiple MicroBooNE measurements of flux-averaged *total* cross sections have included the use of sidebands [133–135]. One of these, a measurement of η meson production [133], used a unique background constraint method that appears to be new to the neutrino cross-section literature. In the remainder of this section, I adapt and generalize this procedure to provide a recipe for incorporating sideband-based refinements to background estimation in MicroBooNE-style measurements of unfolded differential cross sections. I call the generalized technique the *conditional covariance background constraint* (CCBC).

ism of Eq. 60 by either subdividing the background categories \mathfrak{b} in terms of kinematics or by assigning the scale factors bin-independent values $\alpha_{\mathfrak{b}} \rightarrow \alpha_{a\mathfrak{b}}$ as in Ref. [7].

B. Conditional covariance formalism

The mathematical foundation for the CCBC is the conditional multivariate Gaussian distribution. Let the random vector \mathbf{X} follow a multivariate Gaussian distribution with mean vector $\boldsymbol{\mu}$ and covariance matrix V . Without loss of generality, choose the ordering of the elements of \mathbf{X} such that it can be partitioned into two smaller random vectors

$$\mathbf{X} = \begin{pmatrix} \mathbf{X}_1 \\ \mathbf{X}_2 \end{pmatrix}. \quad (61)$$

The mean vector and covariance matrix can thus be written in the form

$$\boldsymbol{\mu} = \begin{pmatrix} \boldsymbol{\mu}_1 \\ \boldsymbol{\mu}_2 \end{pmatrix}, \quad (62)$$

and

$$V = \begin{pmatrix} V_{11} & V_{12} \\ V_{21} & V_{22} \end{pmatrix} \quad (63)$$

respectively. By construction, $V_{12} = V_{21}^T$, and \mathbf{X}_1 (\mathbf{X}_2) follows a multivariate Gaussian distribution with mean $\boldsymbol{\mu}_1$ ($\boldsymbol{\mu}_2$) and covariance matrix V_{11} (V_{22}). Given the observation that the elements of \mathbf{X}_2 have some definite values \mathbf{d}_2 , the conditional probability distribution $P(\mathbf{X}_1 | \mathbf{X}_2 = \mathbf{d}_2)$ of \mathbf{X}_1 is multivariate Gaussian with mean

$$\boldsymbol{\mu}_1^{\text{constr}} = \boldsymbol{\mu}_1 + V_{12} \cdot V_{22}^{-1} \cdot (\mathbf{d}_2 - \boldsymbol{\mu}_2), \quad (64)$$

and covariance matrix

$$V_{11}^{\text{constr}} = V_{11} - V_{12} \cdot V_{22}^{-1} \cdot V_{21}. \quad (65)$$

A proof in which the results from Eqs. 64–65 are derived is given in Ref. [136].

C. Application to low-energy excess analyses

A primary motivation for the MicroBooNE experiment was the observation by LSND [137–140] and MiniBooNE [141, 142] of an anomalous excess of electron (anti)neutrino candidate events at low energies. In all of MicroBooNE’s first analyses investigating possible explanations for the excess, including true ν_e appearance [143–146] and an unexpectedly large rate of neutral-current Δ baryon production followed by radiative decay [147], the conditional covariance formalism from the previous subsection played a major role. Since the presence or absence of an LSND/MiniBooNE-like low-energy excess could only be judged relative to an expectation derived from simulation, robust predictions for the selected event rates were an essential ingredient for interpretation of the measurements.

MicroBooNE's strategy for bolstering confidence in their simulation predictions involved both global improvements adopted for general collaboration use⁶ as well as analysis-specific model constraints. Each of the specific constraints assumed that the expected event counts in the signal region and one or more control samples jointly followed a multivariate Gaussian distribution. The mean of this distribution was taken to be the central-value prediction of the nominal simulation, and the systematic portion of the covariance matrix was evaluated as in Eq. 17, except that there was no special treatment (see Eq. 18) for the interaction model uncertainties. By conditioning on the measured event counts in each of the control sample bins and applying Eqs. 64–65, a refined signal-region prediction with a smaller uncertainty was obtained and used to evaluate the final results.

D. Application to η production measurement

The MicroBooNE analysis reported in Ref. [133] measured a flux-averaged total cross section for neutrino-induced η production. Since the event selection relied upon identification of photon pairs with kinematics consistent with the decay $\eta \rightarrow \gamma\gamma$, photons arising from neutral pion decays represented the dominant source of background. To provide a data-driven constraint of this background, the single bin used to accumulate candidate signal events was supplemented with two control sample bins. The first (second) control sample bin used a modified selection to enhance the contribution from events containing exactly one (two or more) π^0 in the final state.

Inspired by the conditional covariance technique used in the low-energy excess analyses, a similar approach was used to obtain updated estimates for the single- and multi- π^0 background contributions in the signal region. In this case, each of these two dominant backgrounds is constrained individually using the appropriate control sample bin. Let B_{β}^S denote the expected number of background events of type β (either single- or multi- π^0) in the signal region bin. The constrained prediction for this quantity used in Ref. [133] was calculated via an expression equivalent to

$$B_{\beta}^{S,\text{constr}} = B_{\beta}^S + \frac{\text{Cov}(B_{\beta}^S, B_{\beta}^C)}{\text{Var}(B_{\beta}^C)} \cdot (D^C - n^C). \quad (66)$$

In the control sample bin of interest, B_{β}^C is the expected number of background events of type β , D^C is the measured total number of events, and n^C is the total number of events of all kinds predicted by the nominal simulation.

The covariance $\text{Cov}(B_{\beta}^S, B_{\beta}^C)$ and variance

$$\text{Var}(B_{\beta}^C) = \text{Cov}(B_{\beta}^C, B_{\beta}^C) \quad (67)$$

were calculated using an expression similar to Eq. 17 except that only background events of type β were included rather than all events.

By analogy with Eq. 65, the uncertainty on the constrained background prediction in the signal region was represented by the variance

$$\text{Var}(B_{\beta}^{S,\text{constr}}) = \text{Var}(B_{\beta}^S) - \frac{[\text{Cov}(B_{\beta}^S, B_{\beta}^C)]^2}{\text{Var}(B_{\beta}^C)}. \quad (68)$$

This procedure was repeated twice to obtain updated predictions and uncertainties for both the single- and multi- π^0 backgrounds in the signal region.

Although innovative as a first application of the conditional covariance formalism to a sideband-based background constraint for a neutrino cross-section measurement, the approach adopted for the MicroBooNE η production result has some limitations that must be addressed to create a more general technique. First, the expressions given in Eqs. 66 and 68 are appropriate only for a single-bin analysis. However, adapting them for a multi-bin measurement is straightforward in light of the matrix notation used in Eqs. 64 and 65. Second, the η analysis considers each class of background β in isolation from the others and the signal, which neglects potentially important relationships between event categories in the general case. Third, while the present approach provides a recipe for updating the background prediction and its uncertainty in the signal region, the Wiener-SVD unfolding technique favored by MicroBooNE requires an input covariance matrix describing the uncertainty on the *total* event counts (both signal and background) in each reconstructed bin. Due to systematic uncertainties that may be strongly correlated between signal and background events (e.g., those due to the neutrino flux model), one cannot simply assume that the constraint procedure will leave the signal contribution to the total covariance matrix unchanged. The CCBC procedure described below removes all three of these limitations.

E. Assumption of joint Gaussian distribution

In the MicroBooNE approach to cross-section extraction, a covariance matrix $\text{Cov}(n_a, n_b)$ is constructed that describes the uncertainty on the expected event counts n_a in each reconstructed bin a (Sec. II B 2). The multiple-universe expression (Eq. 17) used to evaluate the covariance matrix elements is based on the assumption that the n_a jointly follow a multivariate Gaussian distribution with the mean values given by the central-value prediction n_a^{CV} from the nominal simulation. This description is also compatible with a somewhat more stringent assumption that will form the basis of the CCBC.

⁶ An example is the “MicroBooNE Tune” [86] of the GENIE neutrino event generator.

Divide the expected event counts into signal (ϕ_a) and background (B_a) contributions:

$$n_a = \phi_a + B_a. \quad (69)$$

The covariance matrix element can thus also be subdivided according to

$$\begin{aligned} \text{Cov}(n_a, n_b) &= \text{Cov}(\phi_a, \phi_b) + \text{Cov}(\phi_a, B_b) \\ &\quad + \text{Cov}(B_a, \phi_b) + \text{Cov}(B_a, B_b). \end{aligned} \quad (70)$$

By substituting the right-hand side of Eq. 69 into Eq. 17, one may obtain separate multiple-universe expressions for each term on the right-hand side of Eq. 70. For example,

$$\text{Cov}(\phi_a, B_b) = \frac{1}{N_{\text{univ}}} \sum_{u=1}^{N_{\text{univ}}} (\phi_a^u - \phi_a^{\text{CV}})(B_b^u - B_b^{\text{CV}}). \quad (71)$$

To follow the MicroBooNE prescription for handling neutrino interaction model uncertainties, the signal prediction in the u -th alternate universe ϕ_a^u should be computed as in Eq. 18. That is, for any alternate universe u in which the neutrino interaction model is varied,

$$\phi_a^u = \sum_{\mu} \Delta_{a\mu}^u \phi_{\mu}^{\text{CV}}, \quad (72)$$

where the response matrix elements $\Delta_{a\mu}^u$ are evaluated in the u -th universe, ϕ_{μ}^{CV} is the central-value prediction for the number of signal events in the μ -th true bin, and the sum runs over all true bins in the block of interest (see Sec. III C 2).

As demonstrated above, the total covariance matrix $\text{Cov}(n_a, n_b)$ is separable into components describing the uncertainty on the signal, the background, and their covariances with each other. The individual components are calculable using essentially the same procedure as the combined matrix, which is based on an assumption of joint Gaussianity of the n_a . I will therefore assume that the signal and background event counts (as opposed to just their sums n_a) are jointly multivariate Gaussian random variables with means given by the central-value predictions ϕ_a^{CV} and B_a^{CV} , respectively.

F. Generalized constraint

To adapt the background constraint strategy from Ref. [133] to be suitable for MicroBooNE-style cross-section extraction, updated predictions for both the expected background B_a and the total covariance matrix $\text{Cov}(n_a, n_b)$ must be obtained from the procedure. This can be accomplished by simultaneously conditioning the total (\mathbf{n}_S) and the background-only (\mathbf{B}_S) vectors of predicted event counts in the signal region on the measurement (\mathbf{D}_C) in the control sample bins.

The procedure for doing so is well-defined thanks to

the assumption of joint Gaussianity of both signal and background discussed in the previous section. From this assumption, it is shown in Appendix B that the elements of the combined vector

$$\mathbf{Y} \equiv \begin{pmatrix} \mathbf{n}_S \\ \mathbf{B}_S \\ \mathbf{n}_C \end{pmatrix} \quad (73)$$

are jointly multivariate Gaussian with means equal to their central values (\mathbf{n}_S^{CV} , \mathbf{B}_S^{CV} , \mathbf{n}_C^{CV}) and with the covariance matrix

$$\mathbf{V}_{\mathbf{Y}\mathbf{Y}} = \begin{pmatrix} V_{\mathbf{n}_S\mathbf{n}_S} & V_{\mathbf{n}_S\mathbf{B}_S} & V_{\mathbf{n}_S\mathbf{n}_C} \\ V_{\mathbf{B}_S\mathbf{n}_S} & V_{\mathbf{B}_S\mathbf{B}_S} & V_{\mathbf{B}_S\mathbf{n}_C} \\ V_{\mathbf{n}_C\mathbf{n}_S} & V_{\mathbf{n}_C\mathbf{B}_S} & V_{\mathbf{n}_C\mathbf{n}_C} \end{pmatrix}. \quad (74)$$

Here $V_{\mathbf{n}_C\mathbf{n}_C}$ is the covariance matrix describing uncertainties on the elements of the vector \mathbf{n}_C of expected total event counts in the control sample bins, $V_{\mathbf{B}_S\mathbf{n}_C} = V_{\mathbf{n}_C\mathbf{B}_S}^T$ is the matrix containing covariances between the elements of \mathbf{B}_S and \mathbf{n}_C , etc. Systematic contributions to each of the component covariance matrices in $V_{\mathbf{Y}\mathbf{Y}}$ are evaluated according to the generalized multiple-universe procedure discussed in the previous subsection. Statistical covariances, especially between elements of \mathbf{n}_S and its background portion \mathbf{B}_S , should be calculated accounting for shared events as described in Sec. III C 1.

As shown in Appendix C, evaluating the conditional joint distribution of \mathbf{n}_S and \mathbf{B}_S on the measured total event counts \mathbf{D}_C in the control sample bins leads to the constrained background prediction

$$\mathbf{B}_S^{\text{constr}} = \mathbf{B}_S^{\text{CV}} + V_{\mathbf{B}_S\mathbf{n}_C} \cdot V_{\mathbf{n}_C\mathbf{n}_C}^{-1} \cdot (\mathbf{D}_C - \mathbf{n}_C^{\text{CV}}) \quad (75)$$

in the signal region. Simplifying to the case of a single background category β and single bins for both the signal region and the control sample, this expression only becomes equivalent to Eq. 66 under the approximation that the contributions of the signal and non- β backgrounds to the control sample are either negligible or exactly known. Using the covariance matrix $V_{\mathbf{B}_S\mathbf{n}_C}$ above thus enables constraints from sidebands in which the background(s) of interest are imperfectly isolated from other kinds of events.

The corresponding constrained prediction for the total event counts in the signal region is given by

$$\mathbf{n}_S^{\text{constr}} = \mathbf{n}_S^{\text{CV}} + V_{\mathbf{n}_S\mathbf{n}_C} \cdot V_{\mathbf{n}_C\mathbf{n}_C}^{-1} \cdot (\mathbf{D}_C - \mathbf{n}_C^{\text{CV}}), \quad (76)$$

with an uncertainty described by the covariance matrix

$$V_{\mathbf{n}_S\mathbf{n}_S}^{\text{constr}} = V_{\mathbf{n}_S\mathbf{n}_S} - V_{\mathbf{n}_S\mathbf{n}_C} \cdot V_{\mathbf{n}_C\mathbf{n}_C}^{-1} \cdot V_{\mathbf{n}_S\mathbf{n}_C}^T. \quad (77)$$

A quality check of the results can be performed by assessing quantitative agreement between the prediction and the signal-region measurement \mathbf{D}_S via the chi-squared statistic before

$$\chi_{\text{pre}}^2 = (\mathbf{D}_S - \mathbf{n}_S^{\text{CV}})^T \cdot V_{\mathbf{n}_S\mathbf{n}_S}^{-1} \cdot (\mathbf{D}_S - \mathbf{n}_S^{\text{CV}}), \quad (78)$$

and after

$$\chi^2_{\text{post}} = (\mathbf{D}_S - \mathbf{n}_S^{\text{constr}})^T \cdot (V_{\mathbf{n}_S \mathbf{n}_S}^{\text{constr}})^{-1} \cdot (\mathbf{D}_S - \mathbf{n}_S^{\text{constr}}). \quad (79)$$

the constraint. Successful application of the CCBC should yield a smaller post-constraint value ($\chi^2_{\text{post}} < \chi^2_{\text{pre}}$) together with an improved description of the signal-region data within smaller uncertainties. Deviations from this expected behavior are symptomatic of deficiencies in the simulation and/or poorly-designed sidebands, either of which may require adjustments to an analysis.

G. Use in cross-section extraction

The constrained background prediction $\mathbf{B}_S^{\text{constr}}$ can be removed from the signal-region data in each reconstructed bin to yield a vector of background-subtracted event counts

$$\mathbf{d} = \mathbf{D}_S - \mathbf{B}_S^{\text{constr}} \quad (80)$$

needed as input for cross-section extraction. The other required inputs for MicroBooNE's approach are the constrained total covariance matrix $V_{\mathbf{n}_S \mathbf{n}_S}^{\text{constr}}$, the detector response matrix (Δ , see Eqs. 10 and 13) and the expected signal event counts in each true bin (ϕ_μ^{CV}). The latter two items may be calculated using the nominal simulation provided that the CCBC does not have a strong impact on the expected signal contribution in the reconstructed bins $\phi_S^{\text{constr}} \approx \phi_S^{\text{CV}}$, where

$$\phi_S^{\text{constr}} = \mathbf{n}_S^{\text{constr}} - \mathbf{B}_S^{\text{constr}}, \quad (81)$$

and

$$\phi_S^{\text{CV}} = \mathbf{n}_S^{\text{CV}} - \mathbf{B}_S^{\text{CV}}. \quad (82)$$

Cases in which ϕ_S^{constr} differs from ϕ_S^{CV} noticeably outside of the prior uncertainties from the covariance matrix

$$V_{\phi_S \phi_S} = V_{\mathbf{n}_S \mathbf{n}_S} - V_{\mathbf{n}_S \mathbf{B}_S} - V_{\mathbf{B}_S \mathbf{n}_S} + V_{\mathbf{B}_S \mathbf{B}_S} \quad (83)$$

deserve special scrutiny. They may require analysis changes before an unfolding based on the nominal simulation inputs Δ and ϕ_μ^{CV} can be considered trustworthy.

Since the T2K extraction procedure allows for control sample bins to be included in the likelihood fit, a background constraint that shares some similarities to the CCBC is already included in their scheme automatically. The formalism presented here offers no special advantage over the existing technique.

For MINERvA-style analyses, since the systematic universes are evaluated on the cross sections obtained during repeated unfoldings rather than on reconstructed event counts (see Sec. II A 2), the covariances from Eq. 74 may not be readily available. However, if the covariance matrices $V_{\mathbf{B}_S \mathbf{n}_C}$ and $V_{\mathbf{n}_C \mathbf{n}_C}$ are computed prior to unfolding, then a background constraint based upon them can

be applied in the following way. When re-extracting the cross section in each systematic universe, subtract a new constrained background prediction computed by making the substitutions $\mathbf{B}_S^{\text{CV}} \rightarrow \mathbf{B}_S^u$ and $\mathbf{n}_C^{\text{CV}} \rightarrow \mathbf{n}_C^u$ in Eq. 75. Here the superscript u indicates that the relevant quantity should be evaluated in the systematic universe of interest u . Apart from this adjustment to background subtraction, the remainder of the extraction workflow proceeds normally. The CCBC in this case serves as an alternative to the various methods for fitting the background scale factors α_b (see Sec. IV A) used in many MINERvA measurements.

V. SUMMARY AND CONCLUSIONS

As neutrino experimentalists continue to seek answers to compelling open questions via increasingly precise measurements, corresponding improvements to the precision of neutrino interaction models and simulations will be essential. For accelerator-based experiments operating at GeV energies, a sizeable literature of neutrino cross-section measurements already exists to guide these improvements, and multiple experiments continue to expand the available data sets at an increasing pace.

Cross-section extraction, a concept central to the large majority of neutrino scattering measurements, describes a family of analysis techniques by which event counts measured by a detector are converted into cross-section results directly comparable to theoretical calculations. While the major approaches to cross-section extraction, as typified herein by the standard strategies from MINERvA, MicroBooNE, and T2K, are superficially similar and share a common goal, their mathematical implementations contain significant differences in unfolding method, uncertainty quantification, and interpretation of the results in light of how flux shape modeling uncertainties are handled [46]. In this paper, I have reviewed these similarities and differences in the hope of spurring further community discussion on best practices for the field.

I have also proposed two techniques intended to advance the state of the art in cross-section extraction methods and thus enhance the power of future measurements to inform neutrino interaction model development. The first technique, blockwise unfolding, seeks to remedy the long-standing omission of correlated uncertainties between separate kinematic distributions reported in the same cross-section data release. The lack of information about such correlations limits the full model discrimination potential of current neutrino data sets, but an uncertainty treatment that makes them available is readily achievable if planned ahead of time. Blockwise unfolding defines a way of organizing and presenting neutrino cross-section measurements that allows inter-distribution covariances to be reported, including the possibility of doing so for distributions obtained from distinct analyses from the same experiment.

The second technique proposed in this paper, the con-

ditional covariance background constraint (CCBC), seeks to improve the precision of the removal of background events in the context of MicroBooNE-like cross-section analyses. In many analyses performed by other experiments, background estimation based upon a nominal simulation prediction is refined in a data-driven way using ancillary measurements known as sidebands. While highly useful for improving the quality of measurements in which background contamination is significant, this general approach has not yet been adopted for any of MicroBooNE’s differential cross section results released to date. Recognizing that this may be due in part to a lack of a clear way to incorporate the use of sidebands in MicroBooNE’s preferred method of cross-section extraction, I build upon an approach first described in Ref. [133] to construct the CCBC as a fully compatible recipe. Although devised primarily to solve a problem specific to MicroBooNE-style measurements, analyses adopting MINERVA-like cross-section extraction may also potentially employ a version of the CCBC as an alternative to the standard method based on fits of normalization scale factors.

VI. ACKNOWLEDGMENTS

I thank the organizers of the October 2023 NuXTract workshop at CERN [132], which helped to catalyze the writing of this article and served as an excellent forum to explore related ideas. I also thank the members of the MicroBooNE cross-section working group for helpful discussions.

This manuscript has been authored by Fermi Research Alliance, LLC under Contract No. DE-AC02-07CH11359 with the U.S. Department of Energy, Office of Science, Office of High Energy Physics.

Appendix A: Wiener-SVD regularization matrix

In the Wiener-SVD method, the regularization matrix is calculated according to the expression [82]

$$A_C = C^{-1} \cdot V_C \cdot W_C \cdot V_C^T \cdot C. \quad (\text{A1})$$

The assisting matrix C determines how A_C relates to a prior prediction of the expected unfolded event counts. Common choices for C include the identity matrix and forms based on estimation of derivatives using finite differences. The matrix V_C is obtained in a two-step procedure. First, Cholesky decomposition is applied to the inverse of a covariance matrix

$$E_{ab} \equiv \text{Cov}(D_a, D_b) \quad (\text{A2})$$

representing the total statistical and systematic uncertainty on the measured event counts. This yields

$$E^{-1} = Q^T \cdot Q \quad (\text{A3})$$

where Q is a lower triangular matrix. Second, singular value decomposition is applied to the matrix

$$G \equiv Q \cdot \Delta \cdot C^{-1} \quad (\text{A4})$$

to obtain

$$G = U_C \cdot D_C \cdot V_C^T. \quad (\text{A5})$$

Here U_C (V_C) is an orthogonal matrix with a number of rows equal to the number of reconstructed (true) bins, while D_C is a diagonal matrix.

To calculate the Wiener filter matrix W_C , a linear transformation \mathbf{g} of a vector ϕ of predicted signal event counts in each true bin

$$\mathbf{g} \equiv V_C^T \cdot C \cdot \phi \quad (\text{A6})$$

is first evaluated. Define the symbol

$$h_\mu \equiv g_\mu d_{\mu\mu}, \quad (\text{A7})$$

where g_μ is the element of \mathbf{g} corresponding to the μ -th true bin, and $d_{\mu\mu}$ is the μ -th diagonal element of D_C . Then one may write the elements $w_{\mu\lambda}$ of W_C in the form

$$w_{\mu\lambda} = \frac{h_\mu^2}{h_\mu^2 + 1} \delta_{\mu\lambda}, \quad (\text{A8})$$

where $\delta_{\mu\lambda}$ is the Kronecker delta.

Appendix B: Joint Gaussianity of the elements of \mathbf{Y}

Define the vector \mathbf{X} in terms of four smaller vectors:

$$\mathbf{X} \equiv \begin{pmatrix} \phi_S \\ \mathbf{B}_S \\ \phi_C \\ \mathbf{B}_C \end{pmatrix}. \quad (\text{B1})$$

Here ϕ_S and \mathbf{B}_S have the same number of elements and respectively denote the signal and background event counts in each reconstructed bin from the signal region. The vectors ϕ_C and \mathbf{B}_C have similar meanings for the reconstructed bins belonging to one or more control samples. There is no restriction on the details of how the control samples are defined nor on the number of blocks used in the signal region.

According to the joint Gaussianity assumption from Sec. IV E, the elements of \mathbf{X} follow a multivariate Gaussian distribution with means equal to their central values

$$\mathbf{X}^{\text{CV}} = \begin{pmatrix} \phi_S^{\text{CV}} \\ \mathbf{B}_S^{\text{CV}} \\ \phi_C^{\text{CV}} \\ \mathbf{B}_C^{\text{CV}} \end{pmatrix} \quad (\text{B2})$$

and with the covariance matrix

$$V_{\mathbf{XX}} = \begin{pmatrix} V_{\phi_S \phi_S} & V_{\phi_S \mathbf{B}_S} & V_{\phi_S \phi_C} & V_{\phi_S \mathbf{B}_C} \\ V_{\mathbf{B}_S \phi_S} & V_{\mathbf{B}_S \mathbf{B}_S} & V_{\mathbf{B}_S \phi_C} & V_{\mathbf{B}_S \mathbf{B}_C} \\ V_{\phi_C \phi_S} & V_{\phi_C \mathbf{B}_S} & V_{\phi_C \phi_C} & V_{\phi_C \mathbf{B}_C} \\ V_{\mathbf{B}_C \phi_S} & V_{\mathbf{B}_C \mathbf{B}_S} & V_{\mathbf{B}_C \phi_C} & V_{\mathbf{B}_C \mathbf{B}_C} \end{pmatrix}. \quad (\text{B3})$$

Here $V_{\phi_S \phi_S}$ is the covariance matrix describing the elements of the ϕ_S vector, $V_{\phi_S \mathbf{B}_C} = V_{\mathbf{B}_C \phi_S}^T$ is the matrix describing covariances between the elements of ϕ_S and \mathbf{B}_C , etc.

Define the auxiliary matrix

$$A \equiv \begin{pmatrix} \mathbf{1}^{SS} & \mathbf{1}^{SS} & \mathbf{0}^{SC} & \mathbf{0}^{SC} \\ \mathbf{0}^{SS} & \mathbf{1}^{SS} & \mathbf{0}^{SC} & \mathbf{0}^{SC} \\ \mathbf{0}^{CS} & \mathbf{0}^{CS} & \mathbf{1}^{CC} & \mathbf{1}^{CC} \end{pmatrix}. \quad (\text{B4})$$

Here $\mathbf{1}$ ($\mathbf{0}$) denotes the identity (zero) matrix. When the first (second) superscript is S , then the matrix has a number of rows (columns) equal to the number of reconstructed bins in the signal region. The superscript C uses the same convention but represents the total number of reconstructed bins in the control sample(s).

Since \mathbf{X} is multivariate Gaussian, it can be shown [148, Result 5.2.5] that the vector \mathbf{Y} given by the linear transformation

$$\mathbf{Y} = A \cdot \mathbf{X} \quad (\text{B5})$$

is also multivariate Gaussian with mean

$$\mathbf{Y}^{\text{CV}} = A \cdot \mathbf{X}^{\text{CV}} \quad (\text{B6})$$

and covariance matrix

$$V_{\mathbf{YY}} = A \cdot V_{\mathbf{XX}} \cdot A^T. \quad (\text{B7})$$

By defining the total event count vectors

$$\mathbf{n}_S = \phi_S + \mathbf{B}_S \quad (\text{B8})$$

and

$$\mathbf{n}_C = \phi_C + \mathbf{B}_C, \quad (\text{B9})$$

one may obtain the simplified expressions for \mathbf{Y} and $V_{\mathbf{YY}}$ shown in Eqs. 73 and 74 from the results above.

Appendix C: Conditional constraint derivation

Define the signal-region vector

$$\mathbf{Z} \equiv \begin{pmatrix} \mathbf{n}_S \\ \mathbf{B}_S \end{pmatrix} \quad (\text{C1})$$

so that \mathbf{Y} and its covariance matrix from Eqs. 73 and 74 may be expressed in the form

$$\mathbf{Y} = \begin{pmatrix} \mathbf{Z} \\ \mathbf{n}_C \end{pmatrix} \quad (\text{C2})$$

and

$$V_{\mathbf{YY}} = \begin{pmatrix} V_{\mathbf{ZZ}} & V_{\mathbf{Zn}_C} \\ V_{\mathbf{n}_C \mathbf{Z}} & V_{\mathbf{n}_C \mathbf{n}_C} \end{pmatrix}. \quad (\text{C3})$$

Note that

$$V_{\mathbf{ZZ}} = \begin{pmatrix} V_{\mathbf{n}_S \mathbf{n}_S} & V_{\mathbf{n}_S \mathbf{B}_S} \\ V_{\mathbf{B}_S \mathbf{n}_S} & V_{\mathbf{B}_S \mathbf{B}_S} \end{pmatrix} \quad (\text{C4})$$

is the covariance matrix for \mathbf{Z} , and

$$V_{\mathbf{Zn}_C} = \begin{pmatrix} V_{\mathbf{n}_S \mathbf{n}_C} \\ V_{\mathbf{B}_S \mathbf{n}_C} \end{pmatrix} = V_{\mathbf{n}_C \mathbf{Z}}^T \quad (\text{C5})$$

contains the covariances between the elements of \mathbf{Z} and \mathbf{n}_C .

One may now obtain the conditional distribution of \mathbf{Z} given the measured total event counts \mathbf{D}_C in the control sample bins. Applying the results from Sec. IV B yields the constrained signal-region prediction

$$\mathbf{Z}^{\text{constr}} = \mathbf{Z}^{\text{CV}} + V_{\mathbf{Zn}_C} \cdot V_{\mathbf{n}_C \mathbf{n}_C}^{-1} \cdot (\mathbf{D}_C - \mathbf{n}_C^{\text{CV}}) \quad (\text{C6})$$

with its corresponding covariance matrix

$$V_{\mathbf{ZZ}}^{\text{constr}} = V_{\mathbf{ZZ}} - V_{\mathbf{Zn}_C} \cdot V_{\mathbf{n}_C \mathbf{n}_C}^{-1} \cdot V_{\mathbf{n}_C \mathbf{Z}}. \quad (\text{C7})$$

Here the superscript CV indicates the central value of the quantity of interest as predicted by the nominal simulation. Substituting the expressions above for \mathbf{Z} , $V_{\mathbf{ZZ}}$, and $V_{\mathbf{Zn}_C}$ in terms of their components into Eqs. C6 and C7 leads immediately to the results given in Eqs. 75–77.

[1] A. B. Balantekin, S. Gardiner, K. Mahn, T. Mohayai, J. Newby, V. Pandey, J. Zettlemoyer, J. Asaadi, M. Be-tancourt, D. A. Harris, A. Norrick, F. Kling, B. Ramson, M. C. Sanchez, T. Fukuda, M. Wallbank, and M. Wurm, Snowmass Neutrino Frontier: Neutrino interaction cross sections (NF06) topical group report, arXiv preprint (2022), [arXiv:2209.06872 \[hep-ex\]](https://arxiv.org/abs/2209.06872).

[2] K. Abe *et al.* (Hyper-Kamiokande proto-collaboration), Hyper-Kamiokande design report, arXiv preprint (2018), [arXiv:1805.04163 \[physics.ins-det\]](https://arxiv.org/abs/1805.04163).

[3] B. Abi *et al.*, DUNE far detector technical design report. Volume I. Introduction to DUNE, *J. Instrum.* **15** (08), T08008, [arXiv:2002.02967 \[physics.ins-det\]](https://arxiv.org/abs/2002.02967).

[4] L. Alvarez-Ruso, M. Sajjad Athar, M. Barbaro, D. Cherdack, M. Christy, P. Coloma, T. Donnelly, S. Dytman, A. de Gouv  a, R. Hill, P. Huber, N. Jachowicz, T. Katori, A. Kronfeld, K. Mahn, M. Martini, J. Mor  n, J. Nieves, G. Perdue, R. Petti, D. Richards, F. S  nchez, T. Sato, J. Sobczyk, and G. Zeller, Neutrino Scattering Theory Experiment Collaboration white pa-

per: Status and challenges of neutrino–nucleus scattering, *Prog. Part. Nucl. Phys.* **100**, 1–68 (2018), arXiv:1706.03621 [hep-ph].

[5] K. Mahn, C. Marshall, and C. Wilkinson, Progress in measurements of 0.1–10 GeV neutrino–nucleus scattering and anticipated results from future experiments, *Annu. Rev. Nucl. Part. Sci.* **68**, 105–129 (2018), arXiv:1803.08848 [hep-ex].

[6] S. Henry *et al.* (MINERvA collaboration), Measurement of electron neutrino and antineutrino cross sections at low momentum transfer, arXiv preprint (2023), arXiv:2312.16631 [hep-ex].

[7] A. Olivier *et al.* (MINERvA collaboration), Measurement of the multineutron $\bar{\nu}_\mu$ charged current differential cross section at low available energy on hydrocarbon, *Phys. Rev. D* **108**, 112010 (2023), arXiv:2310.17014 [hep-ex].

[8] J. Kleykamp *et al.* (MINERvA collaboration), Simultaneous measurement of ν_μ quasielasticlike cross sections on CH, C, H₂O, Fe, and Pb as a function of muon kinematics at MINERvA, *Phys. Rev. Lett.* **130**, 161801 (2023), arXiv:2301.02272 [hep-ex].

[9] T. Cai *et al.* (MINERvA collaboration), Measurement of the axial vector form factor from antineutrino–proton scattering, *Nature* **614**, 48–53 (2023).

[10] M. A. Ramírez *et al.* (MINERvA collaboration), Neutrino-induced coherent π^+ production in C, CH, Fe, and Pb at $\langle E_\nu \rangle \sim 6$ GeV, *Phys. Rev. Lett.* **131**, 051801 (2023), arXiv:2210.01285 [hep-ex].

[11] A. Bercellie *et al.* (MINERvA collaboration), Simultaneous measurement of muon neutrino ν_μ charged-current single π^+ production in CH, C, H₂O, Fe, and Pb targets in MINERvA, *Phys. Rev. Lett.* **131**, 011801 (2023), arXiv:2209.07852 [hep-ex].

[12] D. Ruterbories *et al.* (MINERvA collaboration), Simultaneous measurement of proton and lepton kinematics in quasielasticlike $\nu\mu$ -hydrocarbon interactions from 2 to 20 GeV, *Phys. Rev. Lett.* **129**, 021803 (2022), arXiv:2203.08022 [hep-ex].

[13] A. Bashyal *et al.* (MINERvA collaboration), High-statistics measurement of antineutrino quasielastic-like scattering at $E_\nu \sim 6$ GeV on a hydrocarbon target, *Phys. Rev. D* **108**, 032018 (2023), arXiv:2211.10402 [hep-ex].

[14] M. V. Ascencio *et al.* (MINERvA collaboration), Measurement of inclusive charged-current ν_μ scattering on hydrocarbon at $\langle E_\nu \rangle \sim 6$ GeV with low three-momentum transfer, *Phys. Rev. D* **106**, 032001 (2022), arXiv:2110.13372 [hep-ex].

[15] D. Ruterbories *et al.* (MINERvA collaboration), Measurement of inclusive charged-current ν_μ cross sections as a function of muon kinematics at $\langle E_\nu \rangle \sim 6$ GeV on hydrocarbon, *Phys. Rev. D* **104**, 092007 (2021), arXiv:2106.16210 [hep-ex].

[16] A. Filkins *et al.* (MINERvA collaboration), Double-differential inclusive charged-current ν_μ cross sections on hydrocarbon in MINERvA at $\langle E_\nu \rangle \sim 3.5$ GeV, *Phys. Rev. D* **101**, 112007 (2020), arXiv:2002.12496 [hep-ex].

[17] D. Coplowe *et al.* (MINERvA collaboration), Probing nuclear effects with neutrino-induced charged-current neutral pion production, *Phys. Rev. D* **102**, 072007 (2020), arXiv:2002.05812 [hep-ex].

[18] M. F. Carneiro *et al.* (MINERvA collaboration), High-statistics measurement of neutrino quasielasticlike scattering at 6 GeV on a hydrocarbon target, *Phys. Rev. Lett.* **124**, 121801 (2020), arXiv:1912.09890 [hep-ex].

[19] T. Cai *et al.* (MINERvA collaboration), Nucleon binding energy and transverse momentum imbalance in neutrino–nucleus reactions, *Phys. Rev. D* **101**, 092001 (2020), arXiv:1910.08658 [hep-ex].

[20] T. Le *et al.* (MINERvA collaboration), Measurement of $\bar{\nu}_\mu$ charged-current single π^- production on hydrocarbon in the few-GeV region using MINERvA, *Phys. Rev. D* **100**, 052008 (2019), arXiv:1906.08300 [hep-ex].

[21] D. Ruterbories *et al.* (MINERvA collaboration), Measurement of quasielastic-like neutrino scattering at $\langle E_\nu \rangle \sim 3.5$ GeV on a hydrocarbon target, *Phys. Rev. D* **99**, 012004 (2019), arXiv:1811.02774 [hep-ex].

[22] X. G. Lu *et al.* (MINERvA collaboration), Measurement of final-state correlations in neutrino muon-proton mesonless production on hydrocarbon at $\langle E_\nu \rangle = 3$ GeV, *Phys. Rev. Lett.* **121**, 022504 (2018), arXiv:1805.05486 [hep-ex].

[23] C. E. Patrick *et al.* (MINERvA collaboration), Measurement of the Muon Antineutrino Double-Differential Cross Section for Quasielastic-like Scattering on Hydrocarbon at $E_\nu \sim 3.5$ GeV, *Phys. Rev. D* **97**, 052002 (2018), arXiv:1801.01197 [hep-ex].

[24] A. Mislicev *et al.* (MINERvA collaboration), Measurement of total and differential cross sections of neutrino and antineutrino coherent π^\pm production on carbon, *Phys. Rev. D* **97**, 032014 (2018), arXiv:1711.01178 [hep-ex].

[25] O. Altinok *et al.* (MINERvA collaboration), Measurement of ν_μ charged-current single π^0 production on hydrocarbon in the few-GeV region using MINERvA, *Phys. Rev. D* **96**, 072003 (2017), arXiv:1708.03723 [hep-ex].

[26] M. Betancourt *et al.* (MINERvA collaboration), Direct measurement of nuclear dependence of charged current quasielasticlike neutrino interactions using MINERvA, *Phys. Rev. Lett.* **119**, 082001 (2017), arXiv:1705.03791 [hep-ex].

[27] C. M. Marshall *et al.* (MINERvA collaboration), Measurement of neutral-current K^+ production by neutrinos using MINERvA, *Phys. Rev. Lett.* **119**, 011802 (2017), arXiv:1611.02224 [hep-ex].

[28] C. L. McGivern *et al.* (MINERvA collaboration), Cross sections for ν_μ and $\bar{\nu}_\mu$ induced pion production on hydrocarbon in the few-GeV region using MINERvA, *Phys. Rev. D* **94**, 052005 (2016), arXiv:1606.07127 [hep-ex].

[29] C. M. Marshall *et al.* (MINERvA collaboration), Measurement of K^+ production in charged-current ν_μ interactions, *Phys. Rev. D* **94**, 012002 (2016), arXiv:1604.03920 [hep-ex].

[30] J. Mousseau *et al.* (MINERvA collaboration), Measurement of partonic nuclear effects in deep-inelastic neutrino scattering using MINERvA, *Phys. Rev. D* **93**, 071101 (2016), arXiv:1601.06313 [hep-ex].

[31] P. A. Rodrigues *et al.* (MINERvA collaboration), Identification of nuclear effects in neutrino–carbon interactions at low three-momentum transfer, *Phys. Rev. Lett.* **116**, 071802 (2016), [Addendum: *Phys. Rev. Lett.* **121**, 209902 (2018)], arXiv:1511.05944 [hep-ex].

[32] J. Wolcott *et al.* (MINERvA collaboration), Measurement of electron neutrino quasielastic and quasielasticlike scattering on hydrocarbon at $\langle E_\nu \rangle = 3.6$ GeV,

Phys. Rev. Lett. **116**, 081802 (2016), arXiv:1509.05729 [hep-ex].

[33] T. Le *et al.* (MINERvA collaboration), Single neutral pion production by charged-current $\bar{\nu}_\mu$ interactions on hydrocarbon at $\langle E_\nu \rangle = 3.6$ GeV, Phys. Lett. B **749**, 130–136 (2015), arXiv:1503.02107 [hep-ex].

[34] T. Walton *et al.* (MINERvA collaboration), Measurement of muon plus proton final states in ν_μ interactions on hydrocarbon at $\langle E_\nu \rangle = 4.2$ GeV, Phys. Rev. D **91**, 071301 (2015), arXiv:1409.4497 [hep-ex].

[35] A. Higuera *et al.* (MINERvA collaboration), Measurement of coherent production of π^\pm in neutrino and antineutrino beams on carbon from E_ν of 1.5 to 20 GeV, Phys. Rev. Lett. **113**, 261802 (2014), arXiv:1409.3835 [hep-ex].

[36] B. Eberly *et al.* (MINERvA collaboration), Charged pion production in ν_μ interactions on hydrocarbon at $\langle E_\nu \rangle = 4.0$ GeV, Phys. Rev. D **92**, 092008 (2015), arXiv:1406.6415 [hep-ex].

[37] L. Fields *et al.* (MINERvA collaboration), Measurement of muon antineutrino quasielastic scattering on a hydrocarbon target at $E_\nu \sim 3.5$ GeV, Phys. Rev. Lett. **111**, 022501 (2013), arXiv:1305.2234 [hep-ex].

[38] G. A. Fiorentini *et al.* (MINERvA collaboration), Measurement of muon neutrino quasielastic scattering on a hydrocarbon target at $E_\nu \sim 3.5$ GeV, Phys. Rev. Lett. **111**, 022502 (2013), arXiv:1305.2243 [hep-ex].

[39] W. H. Richardson, Bayesian-based iterative method of image restoration, J. Opt. Soc. Am. **62**, 55–59 (1972).

[40] L. B. Lucy, An iterative technique for the rectification of observed distributions, Astron. J. **79**, 745–754 (1974).

[41] G. D’Agostini, A multidimensional unfolding method based on Bayes’ theorem, Nucl. Instrum. Methods Phys. Res. A **362**, 487–498 (1995).

[42] T. Adye, Unfolding algorithms and tests using RooUnfold, in *PHYSTAT 2011* (CERN, Geneva, 2011) pp. 313–318, arXiv:1105.1160 [physics.data-an].

[43] MINERvA collaboration, UnfoldUtils, GitHub repository, <https://github.com/MinervaExpt/UnfoldUtils> (2023).

[44] B. Messerly *et al.* (MINERvA collaboration), An error analysis toolkit for binned counting experiments, EPJ Web Conf. **251**, 03046 (2021), arXiv:2103.08677 [hep-ex].

[45] M. A. Acero *et al.* (NOvA collaboration), Measurement of the double-differential muon-neutrino charged-current inclusive cross section in the NOvA near detector, Phys. Rev. D **107**, 052011 (2023), arXiv:2109.12220 [hep-ex].

[46] L. Koch and S. Dolan, Treatment of flux shape uncertainties in unfolded, flux-averaged neutrino cross-section measurements, Phys. Rev. D **102**, 113012 (2020), arXiv:2009.00552 [hep-ex].

[47] M. A. Acero *et al.* (NOvA collaboration), Measurement of the ν_e –nucleus charged-current double-differential cross section at $\langle E_\nu \rangle = 2.4$ GeV using NOvA, Phys. Rev. Lett. **130**, 051802 (2023), arXiv:2206.10585 [hep-ex].

[48] M. A. Acero *et al.* (NOvA collaboration), Measurement of ν_μ charged-current inclusive π^0 production in the NOvA near detector, Phys. Rev. D **107**, 112008 (2023), arXiv:2306.04028 [hep-ex].

[49] K. Abe *et al.* (T2K collaboration), Measurements of $\bar{\nu}_\mu$ and $\bar{\nu}_\mu + \nu_\mu$ charged-current cross-sections without de- tected pions or protons on water and hydrocarbon at a mean anti-neutrino energy of 0.86 GeV, Prog. Theor. Exp. Phys. **2021**, 043C01 (2021), arXiv:2004.13989 [hep-ex].

[50] K. Abe *et al.* (T2K collaboration), Measurement of the muon neutrino charged-current single π^+ production on hydrocarbon using the T2K off-axis near detector ND280, Phys. Rev. D **101**, 012007 (2020), arXiv:1909.03936 [hep-ex].

[51] K. Abe *et al.* (T2K collaboration), Measurement of the ν_μ charged-current cross sections on water, hydrocarbon, iron, and their ratios with the T2K on-axis detectors, Prog. Theor. Exp. Phys. **2019**, 093C02 (2019), arXiv:1904.09611 [hep-ex].

[52] K. Abe *et al.* (T2K collaboration), Characterization of nuclear effects in muon-neutrino scattering on hydrocarbon with a measurement of final-state kinematics and correlations in charged-current pionless interactions at T2K, Phys. Rev. D **98**, 032003 (2018), arXiv:1802.05078 [hep-ex].

[53] K. Abe *et al.* (T2K collaboration), First measurement of the ν_μ charged-current cross section on a water target without pions in the final state, Phys. Rev. D **97**, 012001 (2018), arXiv:1708.06771 [hep-ex].

[54] K. Abe *et al.* (T2K collaboration), First measurement of the muon neutrino charged current single pion production cross section on water with the T2K near detector, Phys. Rev. D **95**, 012010 (2017), arXiv:1605.07964 [hep-ex].

[55] K. Abe *et al.* (T2K collaboration), Measurement of double-differential muon neutrino charged-current interactions on C_8H_8 without pions in the final state using the T2K off-axis beam, Phys. Rev. D **93**, 112012 (2016), arXiv:1602.03652 [hep-ex].

[56] K. Abe *et al.* (T2K collaboration), Measurement of the inclusive electron neutrino charged current cross section on carbon with the T2K near detector, Phys. Rev. Lett. **113**, 241803 (2014), arXiv:1407.7389 [hep-ex].

[57] K. Abe *et al.* (T2K collaboration), Measurement of the inclusive ν_μ charged current cross section on carbon in the near detector of the T2K experiment, Phys. Rev. D **87**, 092003 (2013), arXiv:1302.4908 [hep-ex].

[58] A. A. Aguilar-Arevalo *et al.* (MiniBooNE collaboration), Measurement of ν_μ and $\bar{\nu}_\mu$ induced neutral current single π^0 production cross sections on mineral oil at $E_\nu \sim \mathcal{O}(1\text{GeV})$, Phys. Rev. D **81**, 013005 (2010), arXiv:0911.2063 [hep-ex].

[59] A. A. Aguilar-Arevalo *et al.* (MiniBooNE collaboration), Measurement of the neutrino neutral-current elastic differential cross section on mineral oil at $E_\nu \sim 1$ GeV, Phys. Rev. D **82**, 092005 (2010), arXiv:1007.4730 [hep-ex].

[60] A. A. Aguilar-Arevalo *et al.* (MiniBooNE collaboration), First measurement of the muon neutrino charged current quasielastic double differential cross section, Phys. Rev. D **81**, 092005 (2010), arXiv:1002.2680 [hep-ex].

[61] A. A. Aguilar-Arevalo *et al.* (MiniBooNE collaboration), Measurement of ν_μ -induced charged-current neutral pion production cross sections on mineral oil at $E_\nu \in 0.5 - 2.0$ GeV, Phys. Rev. D **83**, 052009 (2011), arXiv:1010.3264 [hep-ex].

[62] A. A. Aguilar-Arevalo *et al.* (MiniBooNE collaboration), Measurement of neutrino-induced charged-

current charged pion production cross sections on mineral oil at $E_\nu \sim 1$ GeV, *Phys. Rev. D* **83**, 052007 (2011), arXiv:1011.3572 [hep-ex].

[63] A. A. Aguilar-Arevalo *et al.* (MiniBooNE collaboration), First measurement of the muon antineutrino double-differential charged-current quasi-elastic cross section, *Phys. Rev. D* **88**, 032001 (2013), arXiv:1301.7067 [hep-ex].

[64] A. A. Aguilar-Arevalo *et al.* (MiniBooNE collaboration), Measurement of the antineutrino neutral-current elastic differential cross section, *Phys. Rev. D* **91**, 012004 (2015), arXiv:1309.7257 [hep-ex].

[65] P. Abratenko *et al.* (MicroBooNE collaboration), First measurement of differential cross sections for muon neutrino charged current interactions on argon with a two-proton final state in the MicroBooNE detector, arXiv preprint (2022), arXiv:2211.03734 [hep-ex].

[66] C. Anderson *et al.* (ArgoNeuT collaboration), First measurements of inclusive muon neutrino charged current differential cross sections on argon, *Phys. Rev. Lett.* **108**, 161802 (2012), arXiv:1111.0103 [hep-ex].

[67] R. Acciarri *et al.* (ArgoNeuT collaboration), Measurements of inclusive muon neutrino and antineutrino charged current differential cross sections on argon in the NuMI antineutrino beam, *Phys. Rev. D* **89**, 112003 (2014), arXiv:1404.4809 [hep-ex].

[68] R. Acciarri *et al.* (ArgoNeuT collaboration), First measurement of electron neutrino scattering cross section on argon, *Phys. Rev. D* **102**, 011101 (2020), arXiv:2004.01956 [hep-ex].

[69] R. Fitzpatrick, *Towards an Improved Neutrino Cross Section Landscape: First Measurements of ν_e -Argon and Monoenergetic ν_μ Interactions*, Ph.D. thesis, Michigan U. (2021).

[70] R. Acciarri *et al.* (ArgoNeuT collaboration), First measurement of the cross section for ν_μ and $\bar{\nu}_\mu$ induced single charged pion production on argon using ArgoNeuT, *Phys. Rev. D* **98**, 052002 (2018), arXiv:1804.10294 [hep-ex].

[71] P. Abratenko *et al.* (MicroBooNE collaboration), First measurement of differential charged current quasielastic-like ν_μ -argon scattering cross sections with the MicroBooNE detector, *Phys. Rev. Lett.* **125**, 201803 (2020), arXiv:2006.00108 [hep-ex].

[72] P. Abratenko *et al.* (MicroBooNE collaboration), First measurement of inclusive muon neutrino charged current differential cross sections on argon at $E_\nu \sim 0.8$ GeV with the MicroBooNE detector, *Phys. Rev. Lett.* **123**, 131801 (2019), arXiv:1905.09694 [hep-ex].

[73] P. Abratenko *et al.* (MicroBooNE collaboration), Measurement of differential cross sections for ν_μ -Ar charged-current interactions with protons and no pions in the final state with the MicroBooNE detector, *Phys. Rev. D* **102**, 112013 (2020), arXiv:2010.02390 [hep-ex].

[74] M. B. Avanzini *et al.*, Comparisons and challenges of modern neutrino-scattering experiments, *Phys. Rev. D* **105**, 092004 (2022), arXiv:2112.09194 [hep-ex].

[75] L. Koch, A response-matrix-centred approach to presenting cross-section measurements, *J. Instrum.* **14** (09), P09013, arXiv:1903.06568 [stat.CO].

[76] P. Abratenko *et al.* (MicroBooNE collaboration), First measurement of inclusive electron-neutrino and antineutrino charged current differential cross sections in charged lepton energy on argon in MicroBooNE, *Phys. Rev. D* **105**, L051102 (2022), arXiv:2109.06832 [hep-ex].

[77] P. Abratenko *et al.* (MicroBooNE collaboration), First measurement of energy-dependent inclusive muon neutrino charged-current cross sections on argon with the MicroBooNE detector, *Phys. Rev. Lett.* **128**, 151801 (2022), arXiv:2110.14023 [hep-ex].

[78] P. Abratenko *et al.* (MicroBooNE collaboration), First double-differential measurement of kinematic imbalance in neutrino interactions with the MicroBooNE detector, *Phys. Rev. Lett.* **131**, 101802 (2023), arXiv:2301.03706 [hep-ex].

[79] P. Abratenko *et al.* (MicroBooNE collaboration), Multidifferential cross section measurements of ν_μ -argon quasielasticlike reactions with the MicroBooNE detector, *Phys. Rev. D* **108**, 053002 (2023), arXiv:2301.03700 [hep-ex].

[80] P. Abratenko *et al.* (MicroBooNE collaboration), Measurement of triple-differential inclusive muon-neutrino charged-current cross section on argon with the MicroBooNE detector, arXiv preprint (2023), arXiv:2307.06413 [hep-ex].

[81] P. Abratenko *et al.* (MicroBooNE collaboration), Measurement of nuclear effects in neutrino-argon interactions using generalized kinematic imbalance variables with the MicroBooNE detector, arXiv preprint (2023), arXiv:2310.06082 [nucl-ex].

[82] W. Tang, X. Li, X. Qian, H. Wei, and C. Zhang, Data unfolding with Wiener-SVD method, *J. Instrum.* **12** (10), P10002–P10002, arXiv:1705.03568 [physics.data-an].

[83] Wiener-SVD-Unfolding, GitHub repository, <https://github.com/BNLIF/Wiener-SVD-Unfolding> (2021).

[84] R. Brun and F. Rademakers, ROOT — An object oriented data analysis framework, *Nucl. Instrum. Methods Phys. Res. A* **389**, 81–86 (1997).

[85] ROOT Data Analysis Framework, <https://root.cern.ch>.

[86] P. Abratenko *et al.* (MicroBooNE collaboration), New CC0 π GENIE model tune for MicroBooNE, *Phys. Rev. D* **105**, 072001 (2022), arXiv:2110.14028 [hep-ex].

[87] P. Abratenko *et al.* (MicroBooNE collaboration), Differential cross section measurement of charged current ν_e interactions without final-state pions in MicroBooNE, *Phys. Rev. D* **106**, L051102 (2022), arXiv:2208.02348 [hep-ex].

[88] J. Bourbeau, *Measuring the cosmic-ray energy spectrum, composition, and anisotropy at PeV scales using the IceCube Observatory*, Ph.D. thesis, Wisconsin U., Madison (2019).

[89] J. Bourbeau and Z. Hampel-Arias, PyUnfold: A Python package for iterative unfolding, *J. Open Source Softw.* **3**, 741 (2018), arXiv:1806.03350 [physics.data-an].

[90] K. Abe *et al.* (T2K collaboration), Measurements of the ν_μ and $\bar{\nu}_\mu$ -induced coherent charged pion production cross sections on ^{12}C by the T2K experiment, arXiv preprint (2023), arXiv:2308.16606 [hep-ex].

[91] K. Abe *et al.* (T2K collaboration), First measurement of muon neutrino charged-current interactions on hydrocarbon without pions in the final state using multiple detectors with correlated energy spectra at T2K, arXiv preprint (2023), arXiv:2303.14228 [hep-ex].

[92] K. Abe *et al.* (T2K collaboration), First T2K measurement of transverse kinematic imbalance in the muon-neutrino charged-current single- π^+ production channel

containing at least one proton, *Phys. Rev. D* **103**, 112009 (2021), arXiv:2102.03346 [hep-ex].

[93] K. Abe *et al.* (T2K collaboration), Simultaneous measurement of the muon neutrino charged-current cross section on oxygen and carbon without pions in the final state at T2K, *Phys. Rev. D* **101**, 112004 (2020), arXiv:2004.05434 [hep-ex].

[94] K. Abe *et al.* (T2K collaboration), Measurement of the charged-current electron (anti-)neutrino inclusive cross-sections at the T2K off-axis near detector ND280, *J. High Energ. Phys.* **10**, 114, arXiv:2002.11986 [hep-ex].

[95] K. Abe *et al.* (T2K collaboration), First combined measurement of the muon neutrino and antineutrino charged-current cross section without pions in the final state at T2K, *Phys. Rev. D* **101**, 112001 (2020), arXiv:2002.09323 [hep-ex].

[96] K. Abe *et al.* (T2K collaboration), First measurement of the charged current $\bar{\nu}_\mu$ double differential cross section on a water target without pions in the final state, *Phys. Rev. D* **102**, 012007 (2020), arXiv:1908.10249 [hep-ex].

[97] K. Abe *et al.* (T2K collaboration), Measurement of inclusive double-differential ν_μ charged-current cross section with improved acceptance in the T2K off-axis near detector, *Phys. Rev. D* **98**, 012004 (2018), arXiv:1801.05148 [hep-ex].

[98] Minuit2, <https://root.cern.ch/doc/master/Minuit2Page.html> (2023).

[99] F. James and M. Roos, Minuit: A system for function minimization and analysis of the parameter errors and correlations, *Comput. Phys. Commun.* **10**, 343–367 (1975).

[100] T2K collaboration, xsLLhFitter, GitLab repository, <https://gitlab.com/cuddandr/xsLLhFitter> (2023).

[101] T2K collaboration, GUNDAM, GitHub repository, <https://github.com/gundam-organization/gundam> (2023).

[102] E. W. Weisstein, Stirling's approximation, From MathWorld—A Wolfram Web Resource. <https://mathworld.wolfram.com/StirlingsApproximation.html>.

[103] J. S. Conway, Incorporating nuisance parameters in likelihoods for multisource spectra, in *Proceedings of the PHYSTAT 2011 Workshop on Statistical Issues Related to Discovery Claims in Search Experiments and Unfolding*, edited by H. B. Prosper and L. Lyons (CERN, Geneva, Switzerland, 2011) pp. 115–120.

[104] R. Barlow and C. Beeston, Fitting using finite Monte Carlo samples, *Comput. Phys. Commun.* **77**, 219–228 (1993).

[105] A. N. Tikhonov, Об устойчивости обратных задач (On the stability of inverse problems), *Doklady Akademii Nauk SSSR* **39**, 195–198 (1943).

[106] D. L. Phillips, A technique for the numerical solution of certain integral equations of the first kind, *J. ACM* **9**, 84–97 (1962).

[107] P. C. Hansen, Analysis of discrete ill-posed problems by means of the L-curve, *SIAM Rev.* **34**, 561–580 (1992).

[108] Relationship between the Hessian and covariance matrix for Gaussian random variables, in *Bayesian Methods for Structural Dynamics and Civil Engineering* (2010) pp. 257–262.

[109] A. A. Aguilar-Arevalo *et al.* (MiniBooNE collaboration), MiniBooNE data releases, arXiv preprint (2021), arXiv:2110.15055 [hep-ex].

[110] M. Betancourt *et al.*, Comparisons and challenges of modern neutrino scattering experiments (TENSIONS2016 report), *Phys. Rep.* **773–774**, 1–28 (2018), arXiv:1805.07378 [hep-ex].

[111] C. Wilkinson *et al.*, Testing charged current quasi-elastic and multinucleon interaction models in the NEUT neutrino interaction generator with published datasets from the MiniBooNE and MINERvA experiments, *Phys. Rev. D* **93**, 072010 (2016), arXiv:1601.05592 [hep-ex].

[112] J. Tena-Vidal *et al.* (GENIE collaboration), Neutrino-nucleus CC0 π cross-section tuning in GENIE v3, *Phys. Rev. D* **106**, 112001 (2022).

[113] T. Katori and M. Martini, Neutrino–nucleus cross sections for oscillation experiments, *J. Phys. G: Nucl. Part. Phys.* **45**, 013001 (2017), arXiv:1611.07770 [hep-ph].

[114] E. S. P. Guerra *et al.*, Using world π^\pm -nucleus scattering data to constrain an intranuclear cascade model, *Phys. Rev. D* **99**, 052007 (2019), arXiv:1812.06912 [hep-ex].

[115] T. Bonus, J. T. Sobczyk, M. Siemaszko, and C. Juszczak, Data-based two-body current contribution to the neutrino-nucleus cross section, *Phys. Rev. C* **102**, 015502 (2020), arXiv:2003.00088 [hep-ex].

[116] P. Stowell *et al.* (MINERvA collaboration), Tuning the GENIE pion production model with MINERvA data, *Phys. Rev. D* **100**, 072005 (2019), arXiv:1903.01558 [hep-ex].

[117] L. Alvarez-Ruso *et al.* (GENIE collaboration), Recent highlights from GENIE v3, *Eur. Phys. J. ST* **230**, 4449–4467 (2021), arXiv:2106.09381 [hep-ph].

[118] C. Andreopoulos *et al.*, The GENIE neutrino Monte Carlo generator, *Nucl. Instrum. Methods Phys. Res. A* **A614**, 87–104 (2010), arXiv:0905.2517 [hep-ph].

[119] R. Fine *et al.* (MINERvA collaboration), Data preservation at MINERvA, arXiv preprint (2022), arXiv:2009.04548 [hep-ex].

[120] M. A. Acero *et al.* (NOvA collaboration), Adjusting neutrino interaction models and evaluating uncertainties using NOvA near detector data, *Eur. Phys. J. C* **80**, 1119 (2020), arXiv:2006.08727 [hep-ex].

[121] C. Green, J. Kowalkowski, M. Paterno, M. Fischler, L. Garren, and Q. Lu, The art framework, *J. Phys.: Conf. Ser.* **396**, 022020 (2012).

[122] U. Mosel and K. Gallmeister, Lepton-induced reactions on nuclei in a wide kinematical regime, arXiv preprint (2023), arXiv:2308.16161 [nucl-th].

[123] U. Mosel, Neutrino event generators: foundation, status and future, *J. Phys. G* **46**, 113001 (2019), arXiv:1904.11506 [hep-ex].

[124] O. Buss, T. Gaitanos, K. Gallmeister, *et al.*, Transport-theoretical description of nuclear reactions, *Phys. Rep.* **512**, 1–124 (2012).

[125] Y. Hayato and L. Pickering, The NEUT neutrino interaction simulation program library, *Eur. Phys. J. Spec. Top.* **230**, 4469–4481 (2021), arXiv:2106.15809 [hep-ph].

[126] Y. Hayato, A neutrino interaction simulation program library NEUT, *Acta Phys. Pol. B* **40**, 2477–2489 (2009).

[127] T. Golan, J. Sobczyk, and J. Źmuda, NuWro: the Wrocław Monte Carlo generator of neutrino interactions, *Nucl. Phys. B - Proc. Suppl.* **229–232**, 499 (2012).

[128] T. Golan, C. Juszczak, and J. T. Sobczyk, Effects of final-state interactions in neutrino-nucleus interactions, *Phys. Rev. C* **86**, 015505 (2012), arXiv:1202.4197 [nucl-th].

[129] C. Juszczak, J. A. Nowak, and J. T. Sobczyk, Simulations from a new neutrino event generator, *Nucl. Phys. B Proc. Suppl.* **159**, 211–216 (2006), proceedings of the 4th International Workshop on Neutrino-Nucleus Interactions in the Few-GeV Region, [arXiv:hep-ph/0512365](https://arxiv.org/abs/hep-ph/0512365).

[130] J. Isaacson, W. I. Jay, A. Lovato, P. A. N. Machado, and N. Rocco, Introducing a novel event generator for electron-nucleus and neutrino-nucleus scattering, *Phys. Rev. D* **107**, 033007 (2023), [arXiv:2205.06378 \[hep-ph\]](https://arxiv.org/abs/2205.06378).

[131] J. Isaacson, S. Höche, D. Lopez Gutierrez, and N. Rocco, Novel event generator for the automated simulation of neutrino scattering, *Phys. Rev. D* **105**, 096006 (2022), [arXiv:2110.15319 \[hep-ph\]](https://arxiv.org/abs/2110.15319).

[132] NuXTract – Towards a consensus in neutrino cross sections, Workshop at CERN, October 2–6, <https://indico.cern.ch/event/1302529/> (2023).

[133] P. Abratenko *et al.* (MicroBooNE collaboration), First measurement of η production in neutrino interactions on argon with MicroBooNE, arXiv preprint (2023), [arXiv:2305.16249 \[hep-ex\]](https://arxiv.org/abs/2305.16249).

[134] P. Abratenko *et al.* (MicroBooNE collaboration), First measurement of quasielastic Λ baryon production in muon antineutrino interactions in the MicroBooNE detector, *Phys. Rev. Lett.* **130**, 231802 (2023), [arXiv:2212.07888 \[hep-ex\]](https://arxiv.org/abs/2212.07888).

[135] P. Abratenko *et al.* (MicroBooNE collaboration), Measurement of neutral current single π^0 production on argon with the MicroBooNE detector, *Phys. Rev. D* **107**, 012004 (2023), [arXiv:2205.07943 \[hep-ex\]](https://arxiv.org/abs/2205.07943).

[136] M. L. Eaton, The normal distribution on a vector space, in *Multivariate statistics: A vector space approach*, IMS Lecture Notes Monogr. Ser., Vol. 53 (2007) pp. 116–119.

[137] A. Aguilar *et al.* (LSND collaboration), Evidence for neutrino oscillations from the observation of $\bar{\nu}_e$ appearance in a $\bar{\nu}_\mu$ beam, *Phys. Rev. D* **64**, 112007 (2001), [arXiv:hep-ex/0104049](https://arxiv.org/abs/hep-ex/0104049).

[138] C. Athanassopoulos *et al.* (LSND collaboration), Results on $\nu_\mu \rightarrow \nu_e$ neutrino oscillations from the LSND experiment, *Phys. Rev. Lett.* **81**, 1774–1777 (1998).

[139] C. Athanassopoulos *et al.* (LSND collaboration), Evidence for $\bar{\nu}_\mu \rightarrow \bar{\nu}_e$ oscillations from the LSND experiment at the Los Alamos Meson Physics Facility, *Phys. Rev. Lett.* **77**, 3082–3085 (1996).

[140] C. Athanassopoulos *et al.*, Candidate events in a search for $\bar{\nu}_\mu \rightarrow \bar{\nu}_e$ oscillations, *Phys. Rev. Lett.* **75**, 2650–2653 (1995).

[141] A. A. Aguilar-Arevalo *et al.* (MiniBooNE collaboration), Search for electron neutrino appearance at the $\Delta m^2 \sim 1 \text{ eV}^2$ scale, *Phys. Rev. Lett.* **98**, 231801 (2007), [arXiv:0704.1500 \[hep-ex\]](https://arxiv.org/abs/0704.1500).

[142] A. A. Aguilar-Arevalo *et al.* (MiniBooNE collaboration), Significant excess of electronlike events in the MiniBooNE short-baseline neutrino experiment, *Phys. Rev. Lett.* **121**, 221801 (2018), [arXiv:1805.12028 \[hep-ex\]](https://arxiv.org/abs/1805.12028).

[143] P. Abratenko *et al.* (MicroBooNE collaboration), Search for an excess of electron neutrino interactions in MicroBooNE using multiple final-state topologies, *Phys. Rev. Lett.* **128**, 241801 (2022), [arXiv:2110.14054 \[hep-ex\]](https://arxiv.org/abs/2110.14054).

[144] P. Abratenko *et al.* (MicroBooNE collaboration), Search for an anomalous excess of charged-current ν_e interactions without pions in the final state with the MicroBooNE experiment, *Phys. Rev. D* **105**, 112004 (2022), [arXiv:2110.14065 \[hep-ex\]](https://arxiv.org/abs/2110.14065).

[145] P. Abratenko *et al.* (MicroBooNE collaboration), Search for an anomalous excess of charged-current quasielastic ν_e interactions with the MicroBooNE experiment using Deep-Learning-based reconstruction, *Phys. Rev. D* **105**, 112003 (2022), [arXiv:2110.14080 \[hep-ex\]](https://arxiv.org/abs/2110.14080).

[146] P. Abratenko *et al.* (MicroBooNE collaboration), Search for an anomalous excess of inclusive charged-current ν_e interactions in the MicroBooNE experiment using Wire-Cell reconstruction, *Phys. Rev. D* **105**, 112005 (2022), [arXiv:2110.13978 \[hep-ex\]](https://arxiv.org/abs/2110.13978).

[147] P. Abratenko *et al.* (MicroBooNE collaboration), Search for neutrino-induced neutral-current Δ radiative decay in MicroBooNE and a first test of the MiniBooNE low energy excess under a single-photon hypothesis, *Phys. Rev. Lett.* **128**, 111801 (2022), [arXiv:2110.00409 \[hep-ex\]](https://arxiv.org/abs/2110.00409).

[148] N. Ravishanker, Z. Chi, and D. K. Dey, Multivariate normal and related distributions, in *A first course in linear model theory* (2021) p. 133, 2nd ed.